Suppression of microRNA Activity in Kidney Collecting Ducts Induces Partial Loss of Epithelial Phenotype and Renal Fibrosis

Sachin Hajarnis,[1] Matanel Yheskel,[1] Darren Williams,[1] Thomas Brefort,[2] Bob Glaudemans,[3] Huguette Debaix,[3] Michel Baum,[1,4] Olivier Devuyst,[3] and Vishal Patel[1]

[1]Division of Nephrology, Department of Internal Medicine, and [4]Division of Nephrology, Department of Pediatrics, University of Texas Southwestern Medical Center, Dallas, Texas; [2]Comprehensive Biomarker Center, Heidelberg, Germany; and [3]Institute of Physiology, University of Zurich, Zurich, Switzerland

ABSTRACT

microRNAs (miRNAs) are sequence-specific inhibitors of post-transcriptional gene expression. The physiologic function of these noncoding RNAs in postnatal renal tubules still remains unclear. Surprisingly, they appear to be dispensable for mammalian proximal tubule (PT) function. Here, we examined the effects of miRNA suppression in collecting ducts (CDs). To conclusively evaluate the role of miRNAs, we generated three mouse models with CD-specific inactivation of key miRNA pathway genes *Dicer*, *Dgcr8*, and the entire Argonaute gene family (*Ago1*, *2*, *3*, and *4*). Characterization of these three mouse models revealed that inhibition of miRNAs in CDs spontaneously evokes a renal tubule injury–like response, which culminates in progressive tubulointerstitial fibrosis (TIF) and renal failure. Global miRNA profiling of microdissected renal tubules showed that miRNAs exhibit segmental distribution along the nephron and CDs. In particular, the expression of miR-200c is nearly 70-fold higher in CDs compared with PTs. Accordingly, miR-200s are downregulated in *Dicer*-KO CDs, its direct target genes *Zeb1*, *Zeb2*, and *Snail2* are upregulated, and miRNA-depleted CDs undergo partial epithelial-to-mesenchymal transition (EMT). Thus, miRNAs are essential for CD homeostasis. Downregulation of CD-enriched miRNAs and the subsequent induction of partial EMT may be a new mechanism for TIF progression.

J Am Soc Nephrol 29: 518–531, 2018. doi: https://doi.org/10.1681/ASN.2017030334

CKD affects millions of Americans. Irrespective of the primary cause, the final common pathway leading to kidney failure in all forms of progressive CKD

Received March 26, 2017. Accepted August 16, 2017.

S.H. and M.Y. contributed equally as first authors.

Present address: Thomas Brefort, Eurofins Medigenomix, Ebersberg, Germany.

Published online ahead of print. Publication date available at www.jasn.org.

Correspondence: Dr. Vishal Patel, Division of Nephrology, Department of Internal Medicine, University of Texas Southwestern Medical Center, 5323 Harry Hines Boulevard, Dallas, TX 75390. Email: vishald.patel@utsouthwestern.edu

Copyright © 2018 by the American Society of Nephrology

Significance Statement

microRNAs (miRNAs), short, non-coding RNAs that inhibit mRNA translation, have been shown to be downregulated in tubulointerstitial fibrosis (TIF), yet they appear to be dispensable for proximal tubule function. This study reports that proximal tubules and collecting ducts exhibit distinct miRNA expression profiles. Suppression of miRNAs in collecting ducts, using three mouse models that lack key enzymes needed for miRNA function, spontaneously induces partial epithelial-to-mesenchymal transition (EMT) and results in progressive TIF and renal failure. Thus, downregulation of collecting duct-enriched miRNAs and the subsequent induction of partial EMT may be a new mechanism for TIF. The results suggest that the collecting duct may play a pivotal role in TIF initiation and progression.

is tubulointerstitial fibrosis (TIF). TIF is characterized by renal tubule atrophy associated with the accumulation of fibroblasts and inflammatory cells and the deposition of extracellular matrix. Downregulation of numerous renal tubule miRNAs is observed in models of TIF.[1–5] Similarly, hypoxia signaling, a key pathogenic pathway that promotes TIF, globally downregulates miRNA biogenesis in kidneys. However, whether miRNA downregulation is sufficient to produce TIF, or if miRNAs are required for normal postnatal renal tubule function, is not entirely clear.

MicroRNAs (miRNAs) are short, noncoding RNAs that regulate the expression of genes at the post-transcriptional level. Biogenesis of miRNAs involves the transcription of the miRNA loci by RNA polymerase II and its associated machinery to produce primary miRNAs (pri-miRNAs).[6,7] The pri-miRNAs are several kilobases in length, have secondary structures, and are capped, spliced, and polyadenylated.[8] Within the nucleus, the pri-miRNAs are processed by the microprocessor complex, which comprises the RNAse III enzyme, DROSHA, and the double-stranded RNA (dsRNA)-binding protein, DiGeorge syndrome critical region 8 (DGCR8).[9,10] The initial recognition of the pri-miRNA by DGCR8 is followed by DROSHA-mediated processing to generate the 60–70-nucleotide (nt) hairpin-shaped precursor miRNAs (pre-miRNAs).[9–13] The pre-miRNAs are exported from the nucleus to the cytoplasm by exportin 5 (XPO5).[14–16] Within the cytoplasm, the pre-miRNAs are processed by a second RNAse III enzyme, DICER1, and the dsRNA binding protein, TRBP (transactivation-responsive RNA-binding protein), to produce the mature, approximately 22-nt miRNA duplexes.[17–20] These miRNA duplexes are further processed by members of the Argonaute (AGO) protein family (AGO1, AGO2, AGO3, or AGO4), which along with other proteins constitute the miRNA-induced silencing complex (miRISC). One strand of the miRNA is retained by the miRISC, where Watson–Crick base-pairing between the miRNA seed sequence and complementary sequences located primarily within the 3′-UTRs of mRNAs results in the inhibition of mRNA translation.[21–23]

The primary objective of our study was to elucidate the physiologic function of miRNAs in kidney tubules. Because deletion of *Dicer* from postnatal mammalian proximal tubules (PT) does not affect PT histology or function,[24] we focused our studies on collecting ducts (CDs). Conditional *Dicer* inactivation is a commonly-used approach to investigate the effects of inhibiting miRNA activity. However, recent studies have uncovered several miRNA-independent functions of DICER1.[25–31] Therefore, in addition to generating CD-specific *Dicer* mutant mice, we also produced mice with CD-specific deletion of *Dgcr8*, to disrupt the upstream miRNA microprocessor complex, and CD-specific deletion of the entire AGO gene family, to disrupt the downstream miRISC. Characterization of these various mouse models conclusively proved that suppression of miRNA activity in CDs spontaneously evokes a CKD-like, tubulointerstitial phenotype. Furthermore, we found that PTs and CDs exhibited distinct miRNA expression patterns and identified miR-200 family members as CD-enriched miRNAs. Additional studies revealed that miR-200 might aid in maintaining CD homeostasis by suppressing mRNA targets that activate epithelial-to-mesenchymal transition (EMT), profibrotic, and proinflammatory pathways.

RESULTS

CD-Specific Inactivation of *Dicer* Produces Progressive Kidney Fibrosis

To study the role of miRNAs in CDs, we began by generating Pkhd1/Cre;*Dicer*$^{F/F}$ (*Dicer*-KO) transgenic mice. *Pkhd1* promoter drives Cre expression in CDs but not in any other parts of the kidney. Extremely sparse Pkhd1-Cre–mediated recombination is observed in CDs at postnatal day (P) 1. Pkhd1-Cre activity is observed in approximately 50% of CDs at P4 and approximately 100% of CDs at P7.[32] To characterize Pkhd1-Cre activity in our mouse strains, we generated Pkhd1/Cre; R26R-EYFP reporter mice, which carry an enhanced yellow fluorescent protein (EYFP) reporter gene that is activated by Pkhd1-Cre–mediated loxP recombination. Consistent with previous studies, we observed that 100% of EYFP^{+} tubules were also positive for aquaporin-2 (AQP2), a CD marker (Supplemental Figure 1). Thus, this approach permitted targeted deletion of *Dicer* specifically from postnatal CDs. Quantitative PCR (Q-PCR) confirmed that the expression of *Dicer* was decreased in kidneys from *Dicer*-KO mice compared with control mice (Figure 1A). H&E staining revealed normal kidney histology at P14, including normal-appearing CDs, in *Dicer*-KO mice (Supplemental Figure 2). To assess CD number, kidney sections from P14 control and *Dicer*-KO mice were stained with AQP2. Quantification revealed that an equal number of AQP2-positive CDs were present in kidneys of 14-day-old control and *Dicer*-KO mice (Supplemental Figure 2). These observations suggested that Pkhd1/Cre-mediated inactivation of *Dicer* did not affect postnatal CD maturation.

Next, to determine whether *Dicer* is required for CD homeostasis in older mice, we monitored a cohort of control and *Dicer*-KO mice for approximately 1 year. Initially, *Dicer*-KO adults appeared healthy and were fertile. However, their median survival was reduced to only 6 months. In comparison, control mice lived well past 1 year (Figure 1B). Gross examination revealed that kidneys from aged *Dicer*-KO mice were small and atrophic (Figure 1C). To characterize this phenotype in more detail, we performed histologic and molecular analyses and measured the renal function of *Dicer*-KO mice at earlier ages. Hematoxylin and eosin (H&E) and PicroSirius Red staining revealed normal kidney histology at P18 (Figure 1D). However, at P21, Q-PCR analysis demonstrated a marked elevation in the expression of kidney tubule injury markers *Kim1* and *Ngal* in *Dicer*-KO kidneys compared with control kidneys (Figure 1, F and G). By P35, patchy interstitial fibrosis surrounding atrophic cortical CDs was observed in *Dicer*-KO kidneys, whereas control kidneys exhibited normal histology (Figure 1D). Furthermore, the expression of several profibrotic

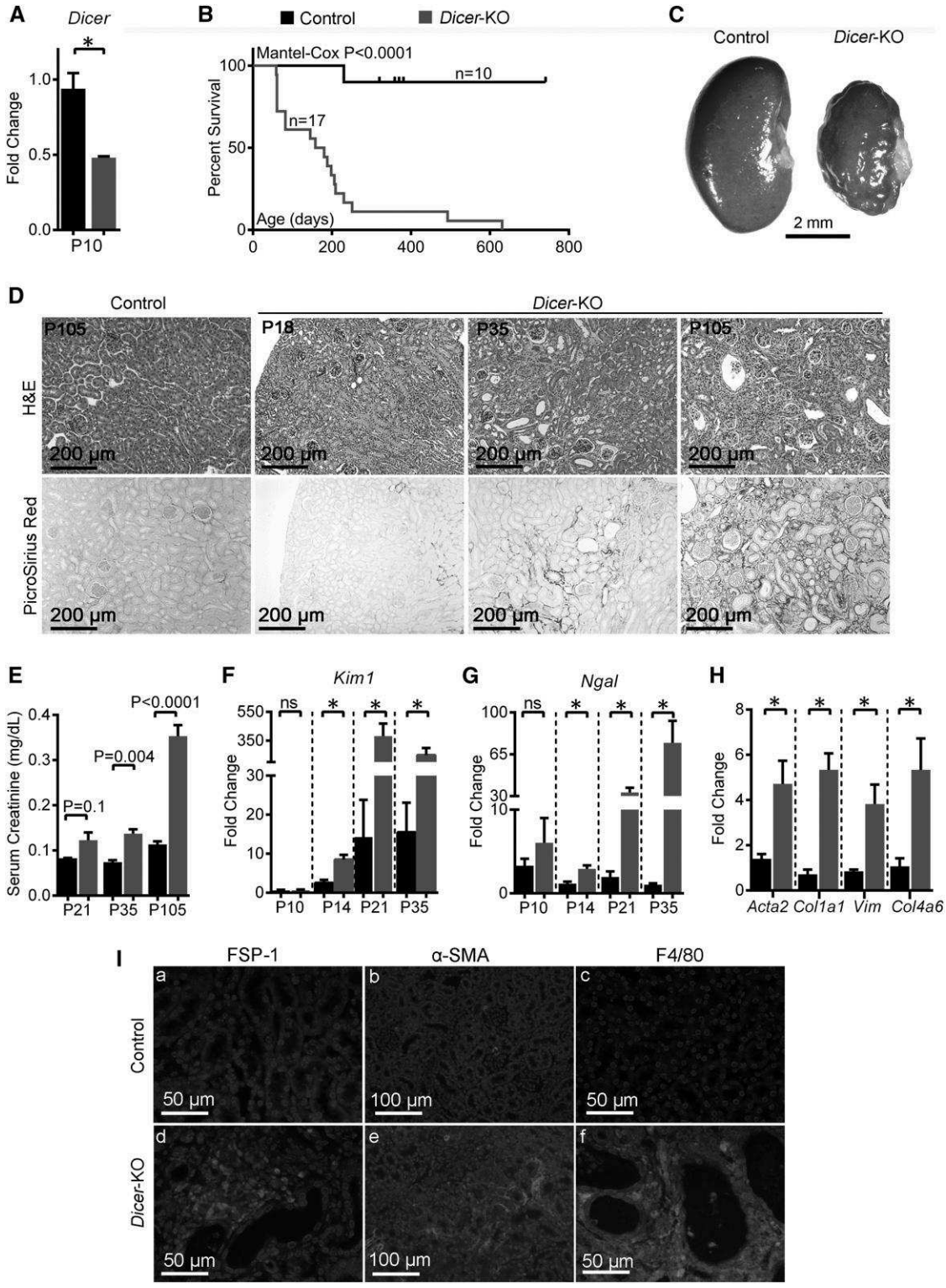

Figure 1. Deletion of *Dicer* from CDs produces progressive kidney fibrosis. (A) Q-PCR established that the expression of *Dicer* was decreased by 50% in kidneys from 10-day-old Pkhd1/Cre;*Dicer*$^{F/F}$ (*Dicer*-KO) mice compared with control mice (n=4). (B) Kaplan–Meier survival curves of *Dicer*-KO and control mice are shown. The median survival of *Dicer*-KO mice was reduced to approximately 6 months. (C) Gross images of kidneys from 280-day-old control and *Dicer*-KO mice are shown. *Dicer*-KO kidneys were smaller and atrophic compared with control kidneys. (D) H&E and PicroSirius Red staining from 35-day-old control mice demonstrated normal glomerular and tubular histology, whereas *Dicer*-KO mice exhibited progressive tubular atrophy and inflammatory infiltrates. (E) Serum

genes (*Acta2*, *Col1a1*, *Vim*, and *Col4a6*) was increased in P35 *Dicer*-KO kidneys compared with control kidneys (Figure 1H). Histologic analysis of kidneys from older *Dicer*-KO mice (P105) revealed that the fibrotic lesions had markedly progressed with age. Accordingly, we observed a progressive rise in serum creatinine levels starting at P35, indicating that kidney fibrosis was associated with reduced renal function in *Dicer*-KO mice (Figure 1E). To further characterize the fibrotic lesions, kidney sections from P35 *Dicer*-KO and control mice were stained with antibodies against fibroblast-specific protein–1 (FSP-1), α–smooth muscle actin (α-SMA), and F4/80, a marker of inflammatory cells. The expression of FSP-1 and α-SMA was increased in the interstitium of *Dicer*-KO kidneys (Figure 1I). Moreover, in addition to fibrosis, immunostaining of *Dicer*-KO kidneys showed infiltration of F4/80$^+$ inflammatory cells within the renal interstitium (Figure 1I). Costaining of FSP-1, α-SMA, and F4/80 with Dolichos Biflorus Agglutinin (DBA), a CD marker, showed that these markers were expressed in interstitial cells surrounding the CDs (Supplemental Figure 3). Interstitial expression of FSP-1, α-SMA, or F4/80 was not observed in control kidneys. Thus, CD-specific inactivation of *Dicer* spontaneously evoked a tubule injury–like response in adult mice, which culminated in renal failure due to progressive interstitial fibrosis and interstitial inflammation.

Deletion of *Dgcr8* from CDs Produces Renal Fibrosis

The DGCR8-DROSHA microprocessor complex catalyzes the first step in the miRNA biogenesis pathway upstream of DICER1 by cleaving pri-miRNA transcripts into smaller pre-miRNAs. As an alternate approach to study the role of miRNAs, we next examined the effects of inhibiting miRNA biogenesis by disrupting the miRNA microprocessor complex in CDs. To address this question, we generated Pkhd1/Cre;*Dgcr8*$^{F/F}$ (*Dgcr8*-KO) mice. Western blot analysis confirmed that the expression of DGCR8 was reduced in kidneys of 35-day-old *Dgcr8*-KO mice compared with control mice (Figure 2A). Gross, histologic, and molecular studies of kidneys from *Dgcr8*-KO mice revealed a striking similarity to kidneys from adult *Dicer*-KO mice. H&E staining of kidney sections from *Dgcr8*-KO mice exhibited normal kidney histology at P14 (Supplemental Figure 2). Moreover, expression of AQP2 and the number of CDs was also similar between P14 control and *Dgcr8*-KO kidneys, indicating that Pkhd1/Cre-mediated deletion of *Dgcr8* did not affect CD maturation (Supplemental Figure 2). However, at P21, Q-PCR analysis revealed a marked increase in the expression of kidney injury markers (*Kim1* and *Ngal*) in *Dgcr8*-KO kidneys compared with control kidneys (Figure 2, F and G). By P35, H&E and PicroSirius Red staining demonstrated cortical CD atrophy and interstitial fibrosis (Figure 2C). Consistent with the histologic studies, Q-PCR analysis showed increased expression of several profibrotic genes in kidneys of 35-day-old *Dgcr8*-KO mice compared with control mice (Figure 2H). Kidneys from approximately 9-month-old *Dgcr8*-KO mice were small and atrophic, and histologic analysis revealed that the fibrotic lesions had significantly worsened (Figure 2, B and D). Serum creatinine levels progressively increased with age, indicating that kidney injury and fibrosis resulted in reduced renal function in *Dgcr8*-KO (Figure 2E).Immunofluorescence staining showed that the expression of FSP-1, α-SMA, and F4/80 was increased in kidneys from *Dgcr8*-KO mice compared with control mice, further indicating that *Dgcr8* deletion resulted in interstitial fibrosis and inflammation (Figure 2I, Supplemental Figure 3). Therefore, deletion of *Dgcr8* from CDs produces a phenotype which is similar to the one observed in *Dicer*-KO mice.

CD-Specific Disruption of the miRISC Results in Kidney Fibrosis

In addition to miRNA biogenesis, both DICER1 and DGCR8 regulate other biologic processes such as DNA damage repair and the generation of snoRNAs and lncRNAs. Thus, the kidney fibrosis phenotype could arise due to miRNA-independent functions of DICER1 and DGCR8. To exclude that possibility, we studied the effects of disrupting the multiprotein miRISC that is essential for the normal miRNA function downstream of DICER1 and DGCR8. Because the AGO protein family members are integral components of the miRISC, we generated mice lacking all AGO proteins in the CDs. The murine AGO proteins (AGO1, AGO2, AGO3, and AGO4) are encoded by four genes located on two distinct genomic loci. The *Ago3*, *1*, and *4* gene cluster is located on chromosome 4, whereas *Ago2* is located on chromosome 15. To study the role of AGO proteins in kidney, we characterized three different mouse models. First, we generated Pkhd1/Cre;*Ago2*$^{F/F}$ (*Ago2*-KO) mice by breeding Pkhd1/Cre mice with *Ago2*$^{F/F}$ mice that harbor loxP sites flanking exons 9–11 of *Ago2*. Q-PCR analysis confirmed that the expression of *Ago2* was decreased in kidneys from *Ago2*-KO mice compared with control mice (Figure 3A). Second, we characterized the *Ago1/3/4*-KO mice, which harbor a germline deletion of the entire *Ago1/3/4* gene cluster. Accordingly, by Q-PCR we observed no expression of Ago1, Ago3, or Ago4 in kidneys of *Ago1/3/4*-KO mice compared with control mice (Figure 3A). Finally, to avoid functional redundancies by the AGO proteins, we generated mice that lacked activity of all

creatinine levels of *Dicer*-KO mice compared with control mice at 3 weeks (P21, n=3–4), 5 weeks (P35, n=3), and 15 weeks of age (P105, n=5–6). (F and G) Q-PCR analysis showed that the expression of kidney injury markers *Kim1* and *Ngal* is increased in kidneys from *Dicer*-KO mice compared with control mice (P10, n=4; P14, n=4; P21, n=6–7; P35, n=3). (H) Q-PCR analysis showed that the expression of the fibrotic markers *Acta2*, *Col1a1*, *Vimentin*, and *Col4a6* was markedly increased in kidneys of 5-week-old *Dicer*-KO mice compared with control mice (n=3). (I) Kidney sections from 5-week-old control and *Dicer*-KO mice were stained with antibodies against FSP-1(green, a and d) and α-SMA (red, b and e), both markers of fibrosis, and F4/80$^+$, a macrophage marker (green, c and f). *Dicer*-KO kidneys showed increased inflammation and interstitial fibrosis compared with control kidneys. Error bars indicate SEM. *P<0.05; ns, P>0.05.

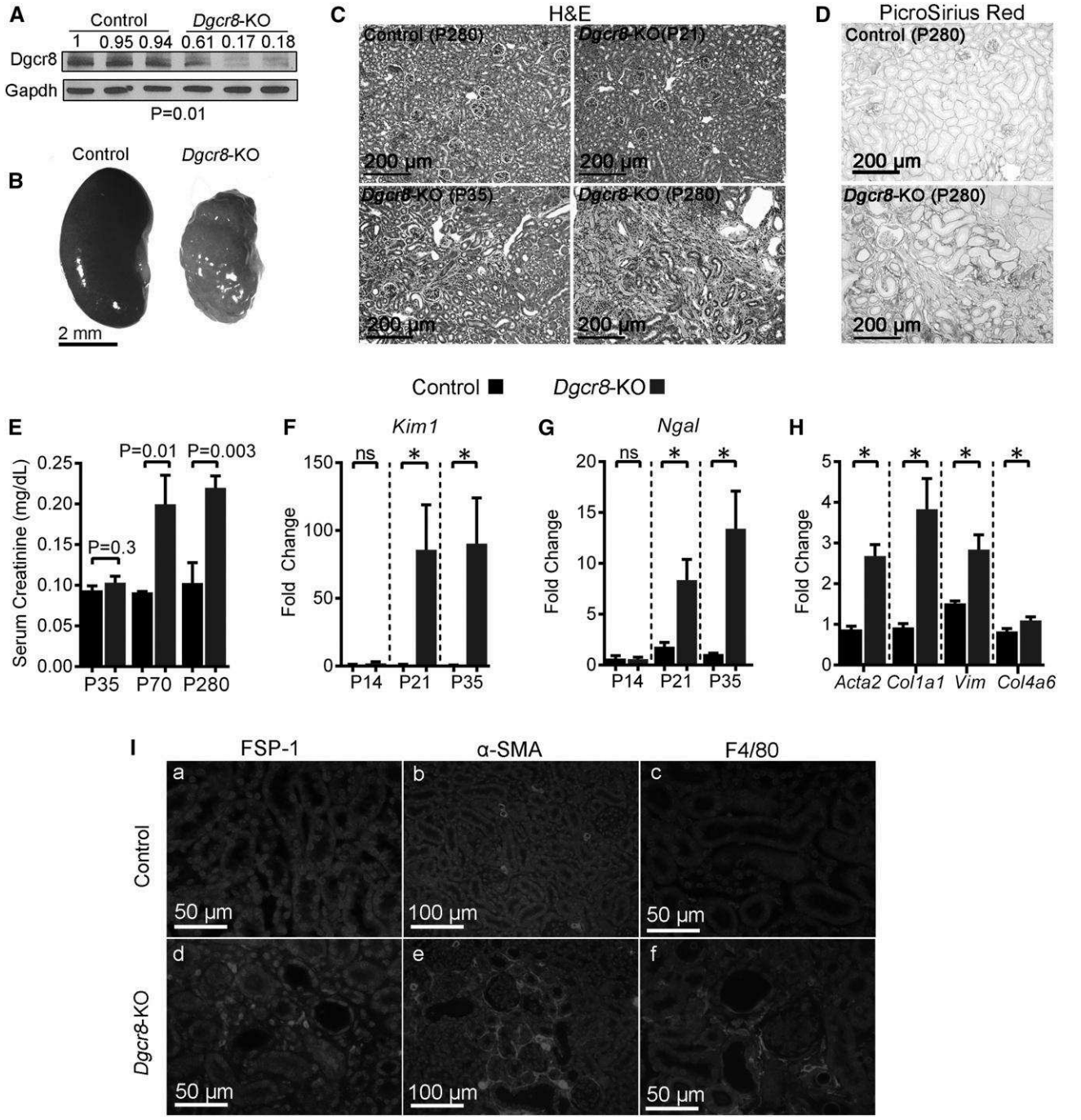

Figure 2. CD-specific deletion of *Dgcr8* results in renal fibrosis. (A) Western blot analysis indicates reduced expression of DGCR8 in kidneys from 35-day-old Pkhd1/Cre;*Dgcr8*$^{F/F}$ (*Dgcr8*-KO) mice. GAPDH was used as a loading control. The protein bands were quantified using Quantity One imaging software from Bio-Rad. (B) Gross kidney images from 280-day-old control and *Dgcr8*-KO mice. *Dgcr8*-KO kidneys were small and atrophic compared with age-matched control kidneys. (C) H&E and (D) PicroSirius Red staining revealed progressive interstitial fibrosis and tubular atrophy in *Dgcr8*-KO mice compared with control mice. (E) Serum creatinine levels were elevated in *Dgcr8*-KO mice compared with control mice (n=4–5). Q-PCR analysis revealed upregulation of kidney injury markers (F) *Kim1* and (G) *Ngal*, indicating progressive renal injury in *Dgcr8*-KO mice compared with controls (P14, n=3; P21, n=3; and P35, n=5). (H) Q-PCR analysis showed that expression of profibrotic genes *Acta2*, *Col1a1*, *Vimentin*, and *Col4a6* was increased in *Dgcr8*-KO mice compared with control mice (n=5–6). (I) Immunostaining of kidney sections from 35-day-old mice showed increased expression of FSP-1 (red, a and d), α-SMA (red, b and e), and F4/80 (green, c and f) in *Dgcr8*-KO mice compared with control mice. Error bars indicate SEM. *P<0.05; ns, P>0.05.

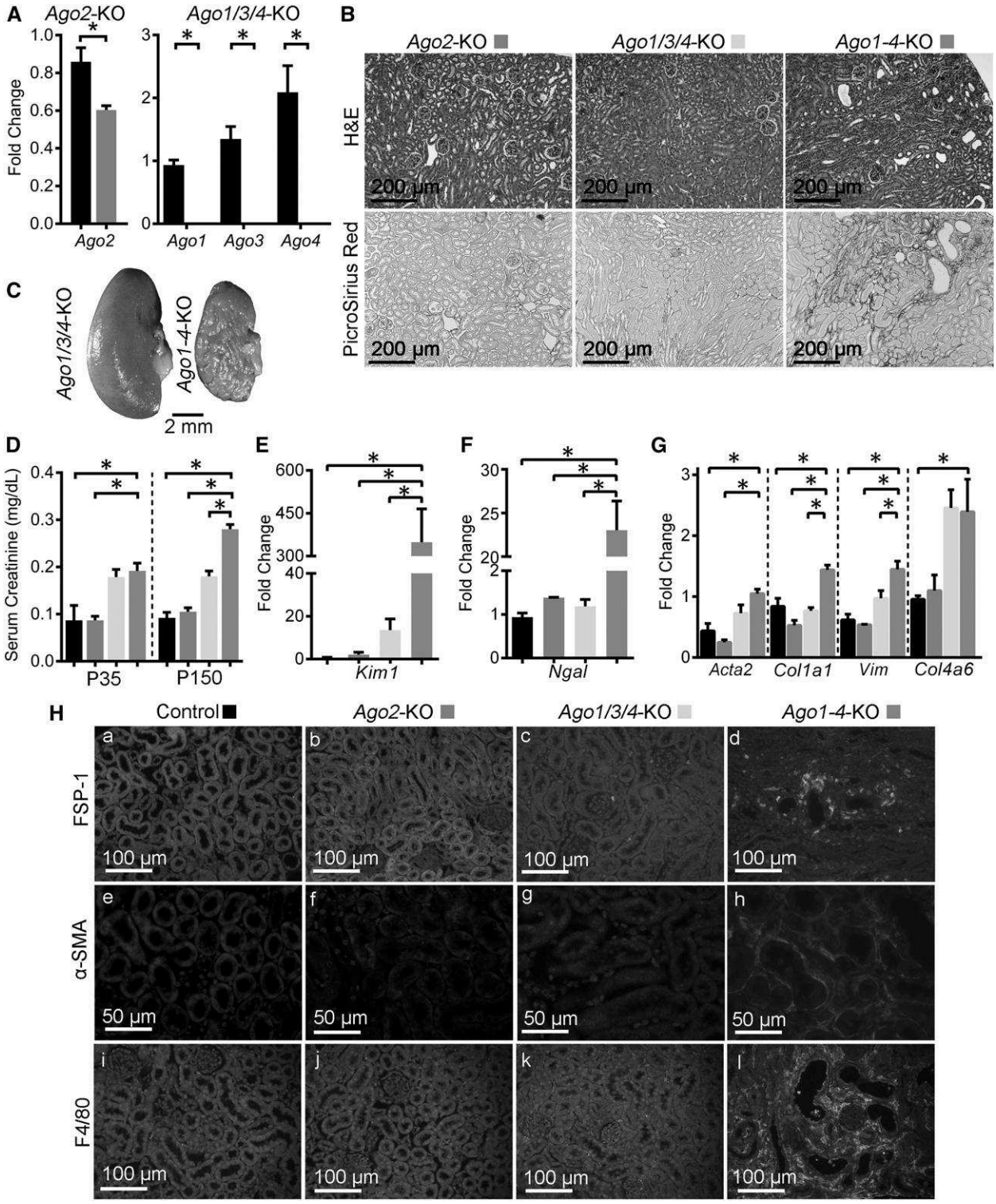

Figure 3. CD-specific disruption of the miRISC recapitulates the fibrotic phenotype of *Dicer*-KO and *Dgcr8*-KO mice. (A) Q-PCR revealed that the expression of *Ago2* was decreased by 30% in kidneys from Pkhd1/Cre;*Ago2*$^{F/F}$ (*Ago2*-KO) mice compared with control mice (n=3). Expression of *Ago1*, *3*, and *4* was ablated in *Ago1/3/4*$^{-/-}$ (n=5–6). (B) H&E and PicroSirius Red staining of kidney sections from 5-week old *Ago2*-KO (Pkhd1/Cre;*Ago2*$^{F/F}$) and *Ago1/3/4*-KO (*Ago1–3-4*$^{-/-}$) mice revealed normal glomerular and kidney histology. In contrast, interstitial fibrosis, inflammation, and tubular atrophy was observed in combined *Ago1–4*-KO mice (*Ago1–3-4*$^{-/-}$; Pkhd1/Cre;*Ago2*$^{F/F}$). (C) Kidneys from 150-day-old *Ago1–4*-KO mice were smaller and atrophic compared with *Ago1/3/4*-KO kidneys. (D) Serum creatinine levels progressively increased in *Ago1–4*-KO mice. Similar progressive increase was not observed in *Ago1/3/4*-KO

four AGO proteins. *Ago1/3/4*-KO mice were crossed with Pkhd1/Cre;*Ago2*$^{F/F}$ (*Ago2*-KO) mice to produce *Ago1/3/4*-KO; Pkhd1/Cre;*Ago2*$^{F/F}$ (*Ago1–4*-KO) mice. *Ago1–4*-KO mice lacked expression of *Ago1*, *Ago3*, and *Ago4* from all tissues, whereas *Ago2* expression was inhibited only in the renal CDs. Both *Ago2*-KO and *Ago1/3/4*-KO mice had normal renal histology and function and exhibited no signs of kidney injury, renal failure, interstitial fibrosis, or the presence of inflammatory cells (Figure 3, B and D–H). In contrast, adult *Ago1–4*-KO mice recapitulated the *Dicer*-KO and *Dgcr8*-KO renal phenotypes. The *Ago1–4*-KO mice exhibited normal kidney histology at P14 (Supplemental Figure 2). However, by P35, atrophic renal tubules and surrounding interstitial fibrosis were observed. Q-PCR analyses revealed that the expression of markers of kidney injury and fibrosis was increased in *Ago1–4*-KO kidneys compared with control, *Ago2-KO*, and *Ago1/3/4*-KO kidneys (Figure 3, E–G). Gross examination revealed that, whereas kidneys from aged *Ago2*-KO and *Ago1/3/4*-KO mice appeared healthy, kidneys from aged (5-month-old) *Ago1–4*-KO mice were small and atrophic, indicating that fibrosis had progressed with age (Figure 3C). Finally, immunofluorescence staining showed increased interstitial expression of FSP-1, α-SMA, and F4/80 in *Ago1–4*-KO kidneys (Figure 3H, Supplemental Figure 3). Interstitial FSP-1, α-SMA, and F4/80 expression was not seen in kidneys from control, *Ago2*-KO, and *Ago1/3/4*-KO mice. Collectively, these results demonstrate that independent deletion of *Ago2* or *Ago1/3/4*-KO gene cluster does not affect CD homeostasis. However, similar to *Dicer* or *Dgcr8* inactivation, combined deletion of all *Ago* genes in CDs produces renal failure due to progressive interstitial fibrosis and interstitial inflammation.

Segmental miRNA Expression Pattern Is Observed along the Nephron and CDs

Although our results have shown that miRNAs play an essential role in CD homeostasis, a previous study found that DICER1 and, by extension, miRNAs are dispensable for PT homeostasis.[24] We reasoned that one potential explanation for these divergent observations may be that CDs and PTs exhibit distinct miRNA expression patterns. Global miRNA expression using RNA extracted from whole kidneys has been previously reported.[33] However, the segmental distribution of miRNAs along the length of the nephron and CD is not known. Therefore, we began by first identifying CD-enriched miRNAs in wild-type kidneys. miRNA microarray analysis was performed using RNA isolated from various nephron segments and CDs. Kidneys from adult wild-type C57 BL/6J mice were sectioned through the midsagittal plane. The cortex and inner medulla were removed, treated with collagenase, and microdissected into various nephron segments, *viz.*, glomerulus (GL), proximal convoluted tubule (PCT), proximal straight tubule (PST), thick ascending limbs (TAL), distal convoluted tubule (DCT), and CDs. Q-PCR analysis of segment-specific marker genes confirmed the purity of each fraction (Supplemental Figure 4). Correlation matrix analysis of the microarray data showed that different biologic samples obtained from the same nephron/CD fractions showed near-identical miRNA expression profiles, further indicating the purity of each fraction (Figure 4A). The complete miRNA expression profile for each nephron segment is shown in Supplemental Table 1. Unsupervised hierarchic clustering of the microarray data revealed that the global miRNA expression profiles segregated into four distinct clusters: GL, PCT/PST, TAL/DCT, and CD (Figure 4B). Expression of ten miRNAs was validated by Q-PCR (miR-143–3p, miR-195a-5p, miR-107–3p, miR-34a-5p, miR-193–3p, miR-378a-5p, miR-874–3p, miR-155–5p, miR-200c-3p, and miR-96–5p). Consistent with the microarray data, Q-PCR analysis also revealed that miRNAs displayed a segmental expression pattern along the nephron and CD (Figure 3C). Next, we identified sixteen high-abundance miRNAs that were expressed at 50% or greater levels in CD compared PCT/PST. Two of these sixteen CD-enriched miRNAs, miR-200c and miR-200a, belong to the miR-200 miRNA family. miR-200c expression was approximately 70-fold enriched in the CD compared with the PTs (Figure 4D). Next, we identified CD-enriched miRNAs that may have contributed to the renal fibrosis phenotype of *Dicer*-KO mice. CD tubules from P18 *Dicer*-KO and control mice were microdissected, and the isolated RNA was used for miRNA microarray analysis (Figure 4E, Supplemental Table 3). Of the 19 miRNAs that showed reduced expression in *Dicer*-KO CDs, three (miR-200c, miR-200a, and miR-429) belonged to the miR-200 family. Intriguingly, miR-200c, which exhibits the highest enrichment in CDs compared with other fractions, was the top downregulated (reduced by approximately 80%) miRNA in *Dicer*-KO CDs compared with control CDs. Furthermore, the expression of other miR-200 family members, miR-200a and miR-429, were reduced by 50% and 33%, respectively, in *Dicer*-KO compared with control CDs (Figure 4E). Thus, these results indicate that the miR-200 members are enriched in the CD, and their expression is significantly reduced when *Dicer* is ablated from the CD.

Suppression of miRNA Activity Induces Partial EMT in CDs

The miR-200 miRNA family members are well known inhibitors of EMT. Recent studies have shown that the induction of partial EMT, a process whereby renal tubule epithelial cells

mice (P35, *n*=3–6; P150, *n*=3–8). (E–G) Q-PCR analyses revealed increased expression of *Kim1* and *Ngal*, and fibrosis markers *Acta2*, *Col1a1*, *Vimentin*, and *Col4a6*, in *Ago1–4*-KO kidneys compared with control, *Ago2*-KO, and *Ago1–3-4*$^{-/-}$ kidneys from 5-week-old mice (*n*=3–6). (H) Kidneys of 5-week-old mice from the indicated models were stained with antibodies against fibrosis marker FSP-1 (green, a–d), α-SMA (red, e–h), and a mouse macrophage marker F4/80^{+} (green, i–l). *Ago1–4*-KO kidneys showed increased inflammation and interstitial fibrosis compared with control, *Ago2-KO*, and *Ago1–3-4*$^{-/-}$ kidneys. Error bars indicate SEM. *$P<0.05$; ns, $P>0.05$.

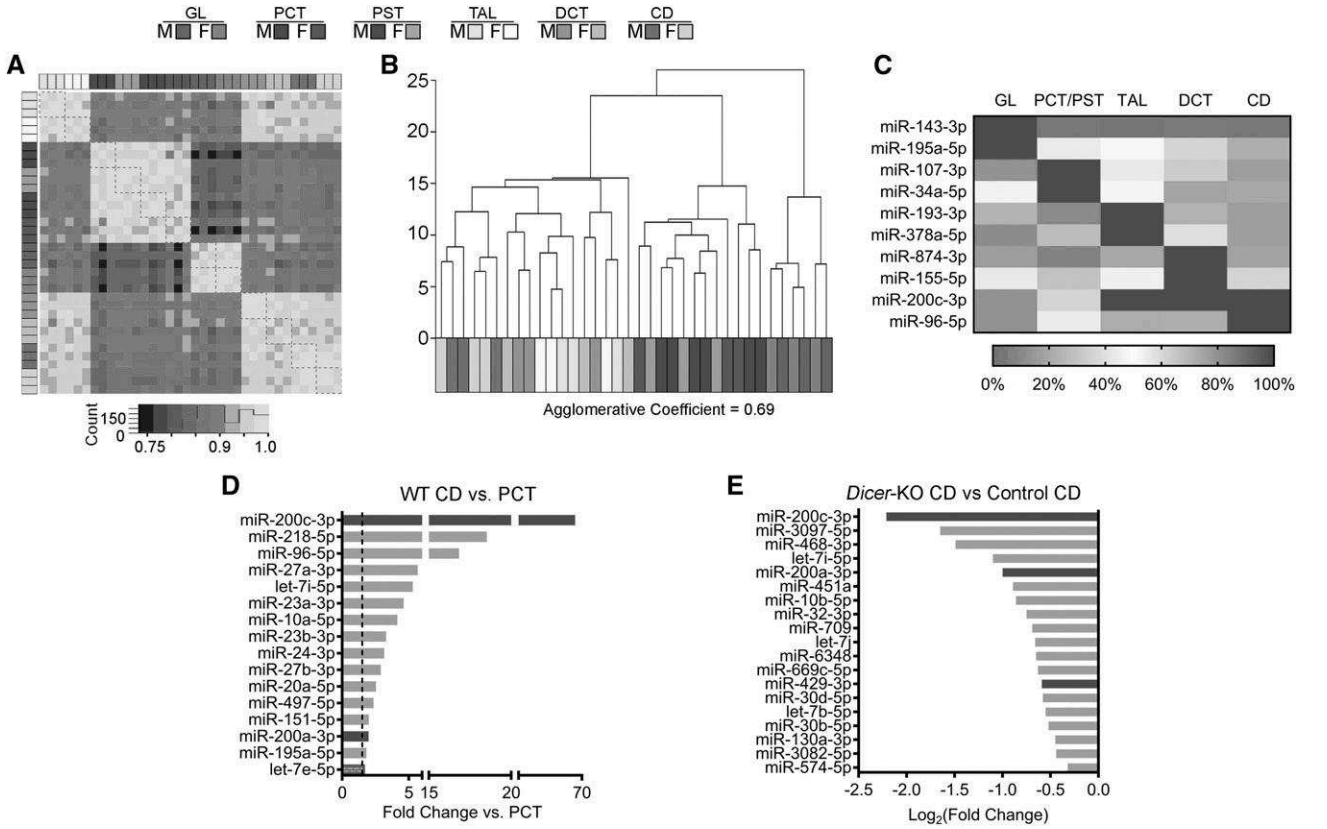

Figure 4. CDs exhibit a distinct miRNA expression profile and show high expression of miR-200 family members. Kidneys from three male and three female wild-type C57 BL/6J mice were microdissected into the following nephron segments: GL, PCT, PST, TAL, DCT, and CD. miRNA microarray analysis was performed using RNA from these segments. (A) Correlation matrix shows the pairwise correlations between all samples. Different biologic samples obtained from the same renal fractions are shown in red dashed boxes. Correlations closer to 1.0 within each of the nephron segment groups indicate high data quality and reproducibility. (B) AGglomerative NESting was used to compute unsupervised agglomerative hierarchic clustering of the nephron segments dataset. The complete dataset was employed, without any additional prior filtering step. Clusters with the shortest average Euclidean distance are combined stepwise. AGglomerative NESting analysis of the miRNA profiles indicates that GL samples form a distinct cluster, whereas PCT and PST samples show no clear separation from each other. Similarly, TAL and DCT samples are not separated from each other but they cluster separately from other groups. The CD group appears as a distinct cluster with some degree of similarity to the TAL/DCT cluster. (C) Consistent with the miRNA microarray data, Q-PCR validation showed that miRNAs exhibit segmental expression pattern. Values are shown as relative expression of the miRNA in various fractions compared with the fraction in which the miRNA is enriched. (D) Sixteen high-abundance miRNAs that were expressed at 50% or greater levels in normal CDs compared with PCTs are shown. miR-200c expression is enriched approximately 68-fold, whereas miR-200a is enriched approximately two-fold in CDs compared with PCT. (E) miRNA microarrays were performed on microdissected CDs from 18-day-old control or *Dicer*-KO mice. Of the 19 miRNAs that showed reduced expression in *Dicer*-KO CDs, three (miR-200c, miR-200a, and miR-429) belonged to the miR-200 family. miR-200c was the top downregulated miRNA with an 80% reduction in expression. F, female; M, male; vs, versus; WT, wild-type.

undergo dedifferentiation and express mesenchymal markers while still retaining the expression of epithelia-related genes, contributes to the progression of kidney fibrosis by promoting inflammation. Therefore, we tested whether downregulation of miR-200 family members was associated with the induction of EMT or partial EMT in CD cells *in vitro* and *in vivo*. Expression of miR-200 was inhibited in a cell line that was derived from mouse inner medullary collecting duct cells (mIMCD3), using locked nucleic acid (LNA)–modified antimiRs against miR-200 family members. Q-PCR analyses revealed that expression of several direct miR-200 targets that promote EMT (*Zeb1*, *Zeb2*, *Snai1*, and *Tgfb2*) was upregulated in anti–miR-200–treated compared with scramble-treated mIMCD3 cells (Figure 5A). In addition, expression of key inflammatory signaling cytokines *Mcp1*, *Il6*, and *Cxcl2* was also elevated in anti–miR-200–treated compared with scramble-treated mIMCD3 cells. However, the expression of two key epithelial-specific genes, *Hnf-1β* and *E-cadherin*, did not change in anti–miR-200–treated compared with scramble-treated cells. To determine whether a similar gene expression pattern was also observed *in vivo*, we analyzed *Dicer*-KO, *Dgcr8*-KO, and *Ago1–4*-KO kidneys. Q-PCR analysis revealed

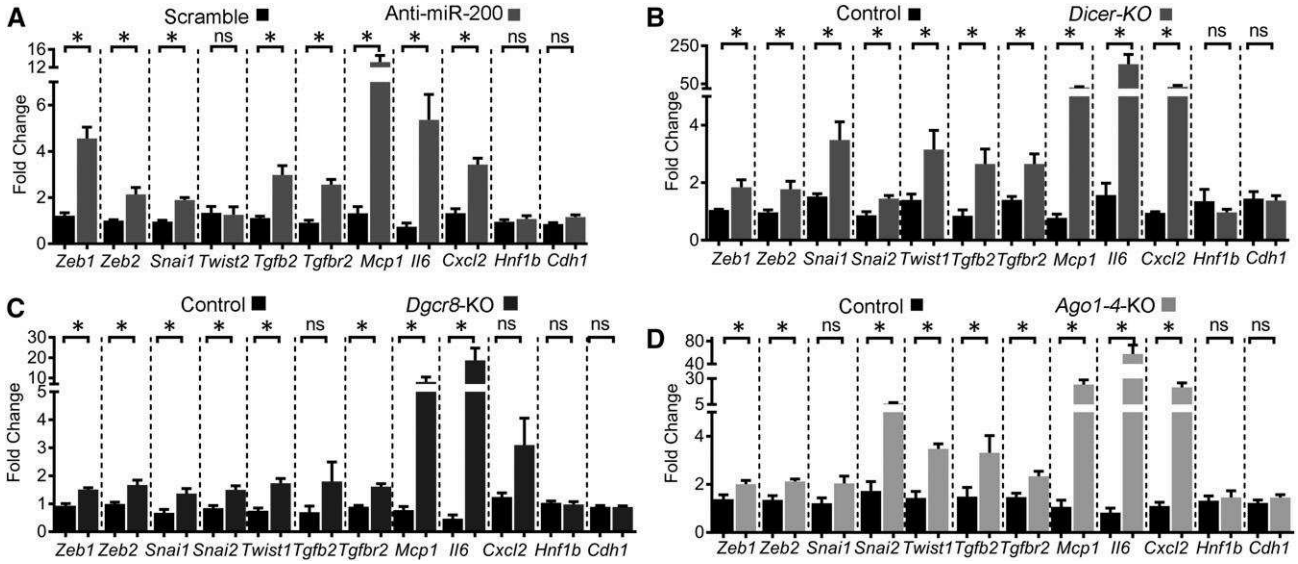

Figure 5. Inhibition of miR-200 activity evokes a profibrotic and inflammatory response. (A) mIMCD3 cells were treated with 10 nM each of LNA-modified anti–miR-200a, anti–miR-200b, and anti–miR-200c to inhibit activity of miR-200 members. Scrambled anti-miR (30 nM)–treated cells were used as controls. Q-PCR analysis indicated increased expression of miR-200-targets and mesenchymal genes *Zeb1*, *Zeb2*, *Snai1*, *Tgfb2*, and *Tgfbr2*, in anti–miR-200–treated cells compared with scramble-treated cells. Expression of inflammatory cytokines *Mcp1*, *Il-6*, and *Cxcl2* was increased, whereas levels of epithelial markers *Hnf1b* and *Cdh1* (E-cadherin) were unchanged in mIMCD3 cells with reduced miR-200 activity. Q-PCR analysis indicated that expression of miR-200 targets, mesenchymal markers, inflammatory genes, and epithelial markers in kidneys from (B) *Dicer*-KO (n=3–4), (C) *Dgcr8*-KO (n=5–6), and (D) *Ago1–4*-KO (n=5–6) mice were similar to that observed in miR-200 knockdown cells. Error bars indicate SEM. *$P<0.05$; ns, $P>0.05$.

that, similar to miR-200 knockdown cells, expression of miR-200 targets *Zeb1*, *Zeb2*, *Snai1*, *Snai2*, and *Tgfb2* and inflammatory cytokines *Mcp1*, *Il6*, and *Cxcl2* was increased, whereas the expression of *Hnf1-β* and *E-cadherin* remained unchanged in *Dicer*-KO, *Dgcr8*-KO, and *Ago1–4*-KO kidneys, compared with their respective control kidneys (Figure 5, B–D).

To test whether EMT was observed *in vivo*, we first examined whether mesenchymal markers are expressed in mutant CDs. Kidney sections from control, *Dicer*-KO, *Dgcr8*-KO, and *Ago1–4*-KO mice were costained with mesenchymal markers Vimentin or SNAIL2 and a CD marker (DBA) or a PT marker Lotus Tetragonolobus Agglutinin (LTA). Expression of both Vimentin and SNAIL2 was observed in DBA-positive CDs in kidneys from *Dicer*-KO, *Dgcr8*-KO, and *Ago1–4*-KO mice but not in kidneys from control mice (Supplemental Figure 5). Similar colocalization was not observed in PTs (Supplemental Figure 6). On the basis of the Q-PCR data, we next tested whether the miRNA-depleted CDs expressed both epithelial and mesenchymal markers. Tubules in kidneys of 35-day-old control mice revealed expression of HNF-1β and E-cadherin (Supplemental Figure 7) but no coexpression of E-cadherin and Vimentin or SNAIL2 (Figure 6). In contrast, tubules in kidneys of 35-day-old *Dicer*-KO, *Dgcr8*-KO, and *Ago1–4*-KO kidneys retained HNF-1β and E-cadherin expression (Supplemental Figure 7) and exhibited coexpression of E-cadherin both with Vimentin and SNAIL2 (Figure 6). The number of Vimentin- and SNAIL2-positive CDs increased in aged (150-day-old) *Dicer*-KO, *Dgcr8*-KO, and *Ago1–4*-KO mice (Figure 6, B and D). As a second approach to examine EMT, we introduced R26R-EYFP reporter in control and *Dicer*-KO mice to perform lineage tracing. We observed that EYFP$^+$ cells in both control and *Dicer*-KO kidney were surrounded by Entactin, a tubular basement membrane marker (Figure 7A). Moreover, we observed no colocalization of EYFP with FSP-1, indicating that *Dicer*-KO CDs remain with the tubular compartment and do not directly contribute to the FSP-1$^+$ cells in the interstitium (Figure 7B). Finally, consistent with our earlier findings, we observed persistent expression of HNF-1β and *de novo* expression of SNAI2 in a subset of EYFP$^+$ tubules in *Dicer*-KO kidneys (Figure 7, C and D). Collectively, these results indicate that suppression of miRNA activity in renal CDs is associated with the induction of partial EMT, which underlies the kidney fibrosis phenotype observed in *Dicer*-KO, *Dgcr8*-KO, and *Ago1–4*-KO mice (Figure 7E).

DISCUSSION

Our study has provided significant new insights into the physiologic function of miRNAs in renal tubules. First, we show that miRNAs are essential for CD homeostasis. miRNAs regulate multiple aspects of embryonic renal tubule development[33] and they have emerged as drug targets for genetic kidney diseases such as autosomal dominant polycystic kidney disease.[34–38] However, the physiologic function of miRNAs in postnatal renal tubules is still unknown. A recent study found that

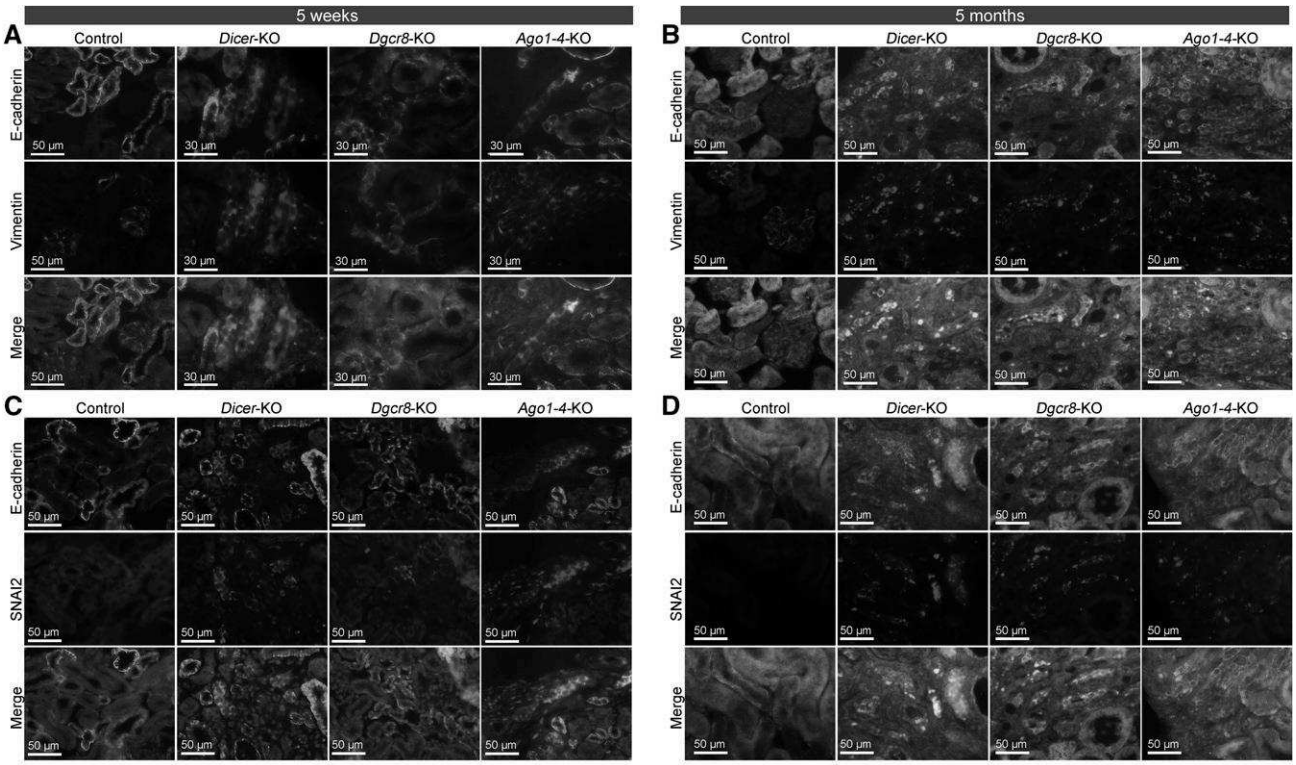

Figure 6. Suppression of miRNA activity induces partial EMT in CDs. Kidney sections from the indicated mouse models at 5 weeks and 5 months of age were costained with antibodies against E-cadherin (green), an epithelial cell junction marker, and mesenchymal markers Vimentin (red) (A and B) or SNAI2 (red) (C and D). The merged panels show colocalization of both the epithelial and mesenchymal markers within kidney tubules.

inactivation of *Dicer* in postnatal PTs does not affect kidney histology or function, suggesting that miRNAs are dispensable for PT homeostasis.[24] In contrast, we found that CD-specific inactivation of *Dicer* spontaneously evoked a renal tubule injury–like response marked by increased levels of injury markers *Ngal* and *Kim1*. Over time, this process culminated into kidney failure due to TIF and inflammation. Although conditional *Dicer* inactivation is a commonly-used approach to investigate the effects of inhibiting miRNA activity, recent studies have shown that DICER1 is a multifaceted enzyme with several other miRNA-independent functions.[25–31] Therefore, in addition to *Dicer* inactivation, we also disrupted the upstream microprocessor and the downstream miRISC. CD-specific disruption of both the microprocessor complex and miRISC recapitulated the kidney fibrosis phenotype of *Dicer*-KO mice, thereby conclusively proving that miRNAs are necessary for CD homeostasis.

The second major insight of our work is that miRNAs aid in CD homeostasis by inhibiting the expression of mRNAs that activate EMT, profibrotic, and proinflammatory pathways. To identify miRNAs that underlie the *Dicer*-KO phenotype, we began by profiling global miRNA expression in microdissected renal tubules. Solely on the basis of miRNA expression profiles, renal tubules can be faithfully divided into three distinct groups (PCT/PST, TAL/DCT, and CD). This observation suggests that kidney miRNAs have unique, segment-specific functions.

We identified miR-200 family members, in particular miR-200c, as CD-enriched miRNAs that may underlie the fibrotic phenotype of our mouse models. A very well described function of the miR-200 family is to repress genes that induce EMT and fibrosis. In keeping with these observations, we found that expression of key activators of EMT and fibrosis (*Zeb1*, *Zeb2*, *Snai1*, *Tgfb2*, *Tgfbr2*) was upregulated in *Dicer*, *Dgcr8*, and *Ago1–4*-KO kidneys as well as miR-200 knockdown cultured CD cells. Moreover, we observed *de novo* expression of mesenchymal markers in CDs of *Dicer*-KO, *Dgcr8*-KO, and *Ago1–4*-KO mice. However, considering that the mutant CD cells remained within the tubular compartment and continued to express epithelial markers, suppression of miRNA activity induced only partial EMT in CDs. Rather than directly generating myofibroblasts, as would be expected if the CDs underwent EMT, the partial EMT CD cells could still promote fibrosis by secreting proinflammatory cytokines. Indeed, expression of proinflammatory cytokines was increased in *Dicer*, *Dgcr8*, and *Ago1–4*-KO kidneys and miR-200 knockdown CD cells. Whether EMT contributes to kidney fibrosis is controversial. However, two recent studies showed that partial EMT is not only observed in renal tubules but is necessary and sufficient to promote inflammation and TIF in mouse models of kidney injury.[39–41]

Finally, our work suggests that dysregulated miRNA expression in CDs might be a new mechanism for the initiation and

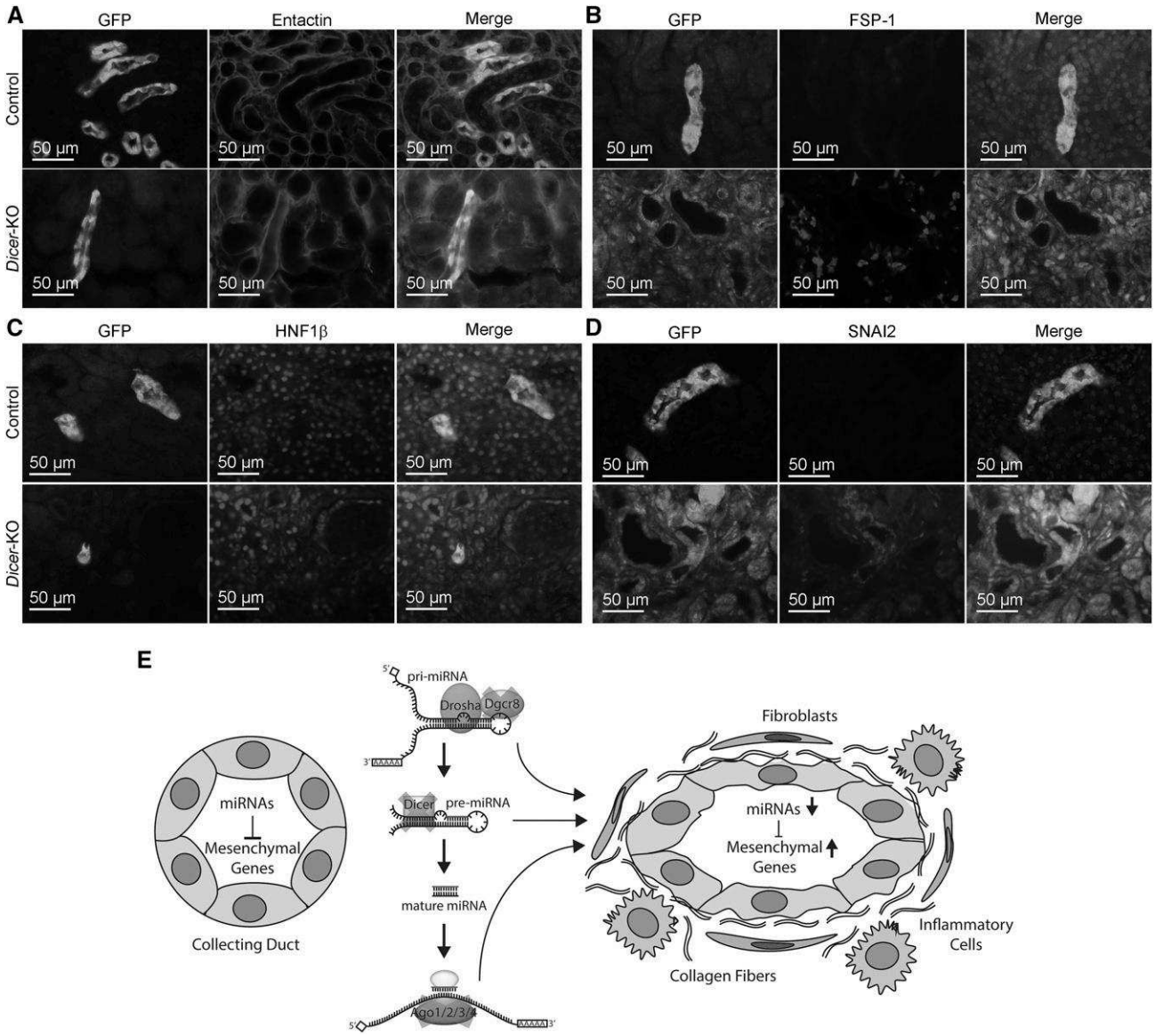

Figure 7. Lineage tracing revealed that *Dicer*-KO CDs undergo partial EMT. Kidney sections from 35-day-old Pkhd1/Cre; R26R-EYFP and *Dicer*-KO; R26R-EYFP mice were costained with antibodies against GFP and (A) Entactin, (B) FSP1, (C) HNF-1β, or (D) SNAI2. EYFP$^+$ tubules in both control and *Dicer*-KO kidneys were surrounded by the basement membrane marker Entactin and did not colocalize with FSP-1. Thus, *Dicer*-KO CDs remained within the tubular compartment and do not directly contribute to FSP-1$^+$ interstitial cells. HNF-1β expression was observed in EYFP$^+$ tubules from control and *Dicer*-KO kidney. *De novo* expression of SNAI2 was observed in a subset of EYFP$^+$ tubules in *Dicer*-KO kidneys, indicating that the mutant CDs exhibit both epithelial and mesenchymal markers suggesting partial EMT. (E) The proposed mechanism is shown.

progression of TIF. Several previous studies have highlighted the fibrogenic potential of CD injury. For example, when exposed to fibrogenic stimuli, CD cells readily undergo EMT.[42,43] Similarly, CDs exhibit partial EMT in the nonhuman primate model of fetal urinary tract obstruction.[44] In murine unilateral urinary tract obstruction models, CDs have been implicated in promoting interstitial inflammation and inhibiting the profibrotic TGF-β signaling.[45,46] However, it is far less clear if CDs can contribute to TIF when the initial site of injury is not within CDs. miR-200c and miR-200a are downregulated in patients with IgA and diabetic nephropathy, respectively[47]—both diseases that initially affect the GL. miR-200c is also downregulated in mouse models of ischemic kidney injury, which primarily affect the PTs.[48,49] Considering that these miRNAs are enriched in CDs and are known to be antifibrotic, the pathogenic effect of their downregulation is likely to be mediated through CDs. Hypoxia signaling, a major pathogenic pathway in TIF, represses *Dicer* in the kidney.[48] Because *Dicer* inactivation in CDs, but not in PTs, recapitulates the phenotype of kidney hypoxia, the pathogenic consequence

of global miRNA downregulation in hypoxia models is also likely to be mediated *via* CDs.

In summary, we have used independent but complementary approaches to examine the physiologic function of miRNAs in CDs. We found that suppression of miRNA activity through CD-specific deletion of key miRNA pathway enzymes results in TIF and renal failure resembling CKD. Global expression profiling revealed marked differences in miRNA expression patterns between the PT and CDs. We identified miR-200 family members as CD-enriched miRNAs and show that downregulation of these miRNAs is associated with partial EMT in the CDs. Thus, our results indicate that miRNAs are essential for CD function. Downregulation of miRNAs and subsequent induction of partial EMT in CDs may be a new general mechanism for TIF progression. Moreover, our work shines a new light into the crucial function of CDs in initiation and progression of TIF.

CONCISE METHODS

Mice

Kidney-specific *Dicer* mutant mice were produced by breeding Pkhd1/Cre mice[50] with *Dicer*$^{F/F}$ mice.[51] The *Dgcr8*$^{F/F}$ (MMRRC stock number: 32051), *Ago2*$^{F/F}$ (JAX stock number: 022558), and Ago3/1/4def (referred to as *Ago1/3/4*-KO mice in the manuscript; JAX stock number: 014152) mice were obtained from Jackson Laboratories. The R26R-EYFP mice were provided by Dr. Frank Costantini (Columbia University). The generation of the following mouse lines is discussed in the Results section: Pkhd1/Cre;*Dgcr8*$^{F/F}$, Pkhd1/Cre;*Ago2*$^{F/F}$, and *Ago1/3/4*-KO;Pkhd1/Cre;*Ago2*$^{F/F}$ (*Ago1–4*-KO). All mice were maintained on a B6 genetic background. All experiments involving animals were conducted under the auspices of the University of Texas Southwestern Medical Center at Dallas and University of Zurich Animal Care and Use Committee.

Tissue Harvesting and Analysis

Mice were anesthetized under approved protocols, blood was obtained by cardiac puncture, and the right kidney was flash frozen for molecular analysis. The left kidney was perfused with cold PBS and 4% (wt/vol) paraformaldehyde and then harvested. Kidneys were fixed with 4% paraformaldehyde for 2 hours, and then embedded in paraffin for sectioning. Sagittal sections of kidneys were stained with H&E or PicroSirius Red for additional analysis.

Renal Function Tests

Serum creatinine was measured using capillary electrophoresis and BUN was measured using the Vitros 250 Analyzer.

Immunofluorescence Staining

The following antibodies and dilutions were used on paraffin-embedded or frozen sections for immunofluorescence staining: anti-GFP (1:400, GFP-1020; Aves), anti-F4/80 (1:50, ab6640; Abcam), anti–α-smooth muscle (1:400, C6198; Sigma-Aldrich), anti-S100A4 (FSP-1) (1:200, ab41532; Abcam), anti-Vimentin (1:100, D21H3; Cell Signaling), anti-SNAIL2 (1:400, C19G7; Cell Signaling), anti-AQP2 (1:400, A7310; Sigma-Aldrich), anti–E-cadherin (1:200, 13–1900; ThermoFisher Scientific), anti–HNF1-β (1:400, sc-22840; SantaCruz Biotechnology). Secondary antibodies were conjugated to Alexa Fluor 488 or Alexa Fluor 594 (1:400; Molecular Probes). Lectins used were Lotus Tetragonolobus Agglutinin (1:300, FL-1321; Vector Laboratories) and DBA (1:200, FL-1031; Vector Laboratories).

Western Blot Analysis

Total protein was extracted from *Dgcr8-KO* and control kidneys. Twenty micrograms of protein was loaded on a 4%–15% SDS-polyacrylamide gel, and the proteins were transferred to a nitrocellulose membrane. The membrane was blocked with 5% milk solution and probed overnight at 4°C with a primary rabbit anti-DGCR8 antibody (1:1000, Abcam 36865). Goat–anti-rabbit HRP-conjugated IgG was used as a secondary antibody, and the blot was developed using the SuperSignal West Dura Extended Duration substrate from Pierce. The protein bands were quantified using Quantity One imaging software from Bio-Rad.

Cell Culture

Mouse inner medullary (mIMCD3) cells were grown in DMEM low-glucose medium supplemented with 10% FBS and maintained in 5% CO2 atmosphere at 37°C. mIMCD3 cells were plated in six-well plates (2×10^5 cells/well) and transfected with 10 nM each of anti–miR-200a, anti–miR-200b, and anti–miR-200c (Exiqon) with Lipofectamine 2000 (Life Technologies). Thirty nanomolar of scrambled anti-miR was used as controls. The cells were harvested 48 hours after transfection and lysed in Qiazol. The sequences of the miR-200 anti-miR and the scramble anti-miRs have been previously published.[33]

RNA Isolation and Quantitative RT-PCR

Total RNA was isolated from cultured cells or mouse kidneys using the miRNeasy Mini kit (Qiagen). First-strand cDNA was synthesized using the SuperScript III Reverse transcription from Life Technologies. Quantitative real-time PCR was performed by loading samples in triplicates on a CFX Connect Real-Time PCR Detection System. We used 18S RNA to normalize gene expression for mRNA, and the data were analyzed using the Bio-Rad CFX software.

Microdissection of Kidney Tubules

Kidney tubules were isolated as previously described.[52] Kidney slices were placed into a prewarmed collagenase type I (1.5 mg/ml dissolved in DMEM/F12; Worthington, Lakewood, NJ) solution in a 15-ml tube, with vigorous shaking at 37°C for 10–15 minutes. After digestion, the individual nephron segments were dissected in 4°C Hank's solution and transferred by adhering the tubules to small glass beads (0.5-mm diameter; Thomas Scientific, Swedesboro, NJ) and then transferring the beads to 1.5-ml tubes containing Qiazol to isolate total RNA.

miRNA Microarrays

Total RNA was isolated from microdissected nephron segments from wild-type kidneys and analyzed using the SurePrint mouse miRNA microarrays (Agilent Technologies). To examine the miRNA expression patterns, total RNA was isolated from microdissected CDs from

Dicer-KO and control mice, with miRNeasy kits, and miRNA microarrays analysis was performed by LC Sciences (Houston, TX) as previously described.[33]

miRNA Isolation and Quantitative Real-Time PCR

The validity of the miRNA microarray results was confirmed by reverse transcription quantitative real-time PCR analysis for two distinct miRNAs (see Supplemental Table 4 for primers) for each of the five nephron segments microdissected from wild-type kidneys. The analysis was obtained in five independent samples, each pooled from six wild-type kidneys. Total RNA was reverse transcribed using miScript II RT kit (QIAGEN). The cDNA (diluted 10×) was used for a 40-cycle Q-PCR reaction with miScript specific Primers (forward primer) and miScript Universal Primers ([reverse primer] sequences proprietary of QIAGEN) with miScript SYBR green PCR KIT (QIAGEN). All reactions were performed on CFX96 Real-Time PCR Detection System (Bio-Rad Laboratories, Hercules, CA). Two endogenous small RNA control targets (RNU6–6P and SNORD61: sequences proprietary of QIAGEN) were used to normalize and the expression values of the respective miRNA were compared using the $\Delta\Delta C_T$ method.

Statistical Analyses

Data are shown as mean±SEM. Statistical analysis was performed using *t* test. ANOVA followed by Dunnett's *post hoc* test was used for multiple comparisons. Log-rank (Mantel–Cox) test was used to compare differences in the survival analyses. $P<0.05$ was considered statistically significant.

ACKNOWLEDGMENTS

We thank the University of Texas Southwestern O'Brien Kidney Research Core Center for providing critical reagents.

The work from the authors' laboratory is supported by National Institutes of Health grants R01DK102572 (to V.P.). These studies were also supported in part by the European Community's Seventh Framework Programme (FP7/2007-2013) under grant agreement no. 246539 (Marie Curie) and grant no. 305608 (EURenOmics), the Swiss National Science Foundation (31003A_169850), and the Rare Disease Initiative Zurich (radiz), a clinical research priority program of the University of Zurich, Switzerland.

DISCLOSURES

None.

REFERENCES

1. Zarjou A, Yang S, Abraham E, Agarwal A, Liu G: Identification of a microRNA signature in renal fibrosis: Role of miR-21. *Am J Physiol Renal Physiol* 301: F793–F801, 2011
2. Wang B, Koh P, Winbanks C, Coughlan MT, McClelland A, Watson A, Jandeleit-Dahm K, Burns WC, Thomas MC, Cooper ME, Kantharidis P: miR-200a prevents renal fibrogenesis through repression of TGF-β2 expression. *Diabetes* 60: 280–287, 2011
3. Xiong M, Jiang L, Zhou Y, Qiu W, Fang L, Tan R, Wen P, Yang J: The miR-200 family regulates TGF-β1-induced renal tubular epithelial to mesenchymal transition through Smad pathway by targeting ZEB1 and ZEB2 expression. *Am J Physiol Renal Physiol* 302: F369–F379, 2012
4. Hajarnis SS, Patel V, Aboudehen K, Attanasio M, Cobo-Stark P, Pontoglio M, Igarashi P: Transcription factor Hepatocyte Nuclear Factor-1β (HNF-1β) regulates microRNA-200 expression through a long noncoding RNA. *J Biol Chem* 290: 24793–24805, 2015
5. Chung AC, Huang XR, Meng X, Lan HY: miR-192 mediates TGF-beta/Smad3-driven renal fibrosis. *J Am Soc Nephrol* 21: 1317–1325, 2010
6. Lee Y, Jeon K, Lee JT, Kim S, Kim VN: MicroRNA maturation: Stepwise processing and subcellular localization. *EMBO J* 21: 4663–4670, 2002
7. Ha M, Kim VN: Regulation of microRNA biogenesis. *Nat Rev Mol Cell Biol* 15: 509–524, 2014
8. Lee Y, Kim M, Han J, Yeom KH, Lee S, Baek SH, Kim VN: MicroRNA genes are transcribed by RNA polymerase II. *EMBO J* 23: 4051–4060, 2004
9. Gregory RI, Yan KP, Amuthan G, Chendrimada T, Doratotaj B, Cooch N, Shiekhattar R: The microprocessor complex mediates the genesis of microRNAs. *Nature* 432: 235–240, 2004
10. Denli AM, Tops BB, Plasterk RH, Ketting RF, Hannon GJ: Processing of primary microRNAs by the microprocessor complex. *Nature* 432: 231–235, 2004
11. Han J, Lee Y, Yeom KH, Kim YK, Jin H, Kim VN: The Drosha-DGCR8 complex in primary microRNA processing. *Genes Dev* 18: 3016–3027, 2004
12. Lee Y, Ahn C, Han J, Choi H, Kim J, Yim J, Lee J, Provost P, Rådmark O, Kim S, Kim VN: The nuclear RNase III Drosha initiates microRNA processing. *Nature* 425: 415–419, 2003
13. Landthaler M, Yalcin A, Tuschl T: The human DiGeorge syndrome critical region gene 8 and Its D. melanogaster homolog are required for miRNA biogenesis. *Curr Biol* 14: 2162–2167, 2004
14. Bohnsack MT, Czaplinski K, Gorlich D: Exportin 5 is a RanGTP-dependent dsRNA-binding protein that mediates nuclear export of pre-miRNAs. *RNA* 10: 185–191, 2004
15. Lund E, Güttinger S, Calado A, Dahlberg JE, Kutay U: Nuclear export of microRNA precursors. *Science* 303: 95–98, 2004
16. Yi R, Qin Y, Macara IG, Cullen BR: Exportin-5 mediates the nuclear export of pre-microRNAs and short hairpin RNAs. *Genes Dev* 17: 3011–3016, 2003
17. Lee HY, Doudna JA: TRBP alters human precursor microRNA processing in vitro. *RNA* 18: 2012–2019, 2012
18. Chendrimada TP, Gregory RI, Kumaraswamy E, Norman J, Cooch N, Nishikura K, Shiekhattar R: TRBP recruits the Dicer complex to Ago2 for microRNA processing and gene silencing. *Nature* 436: 740–744, 2005
19. Tomari Y, Zamore PD: Perspective: Machines for RNAi. *Genes Dev* 19: 517–529, 2005
20. Meister G, Tuschl T: Mechanisms of gene silencing by double-stranded RNA. *Nature* 431: 343–349, 2004
21. Liu J, Valencia-Sanchez MA, Hannon GJ, Parker R: MicroRNA-dependent localization of targeted mRNAs to mammalian P-bodies. *Nat Cell Biol* 7: 719–723, 2005
22. Gregory RI, Chendrimada TP, Cooch N, Shiekhattar R: Human RISC couples microRNA biogenesis and posttranscriptional gene silencing. *Cell* 123: 631–640, 2005
23. Eichhorn SW, Guo H, McGeary SE, Rodriguez-Mias RA, Shin C, Baek D, Hsu SH, Ghoshal K, Villén J, Bartel DP: mRNA destabilization is the dominant effect of mammalian microRNAs by the time substantial repression ensues. *Mol Cell* 56: 104–115, 2014
24. Wei Q, Bhatt K, He HZ, Mi QS, Haase VH, Dong Z: Targeted deletion of Dicer from proximal tubules protects against renal ischemia-reperfusion injury. *J Am Soc Nephrol* 21: 756–761, 2010
25. Nakagawa A, Shi Y, Kage-Nakadai E, Mitani S, Xue D: Caspase-dependent conversion of Dicer ribonuclease into a death-promoting deoxyribonuclease. *Science* 328: 327–334, 2010
26. Kaneko H, Dridi S, Tarallo V, Gelfand BD, Fowler BJ, Cho WG, Kleinman ME, Ponicsan SL, Hauswirth WW, Chiodo VA, Karikó K, Yoo JW, Lee DK, Hadziahmetovic M, Song Y, Misra S, Chaudhuri G, Buaas FW, Braun RE,

Hinton DR, Zhang Q, Grossniklaus HE, Provis JM, Madigan MC, Milam AH, Justice NL, Albuquerque RJ, Blandford AD, Bogdanovich S, Hirano Y, Witta J, Fuchs E, Littman DR, Ambati BK, Rudin CM, Chong MM, Provost P, Kugel JF, Goodrich JA, Dunaief JL, Baffi JZ, Ambati J: DICER1 deficit induces Alu RNA toxicity in age-related macular degeneration. *Nature* 471: 325–330, 2011
27. Wei W, Ba Z, Gao M, Wu Y, Ma Y, Amiard S, White CI, Rendtlew Danielsen JM, Yang YG, Qi Y: A role for small RNAs in DNA double-strand break repair. *Cell* 149: 101–112, 2012
28. Francia S, Michelini F, Saxena A, Tang D, de Hoon M, Anelli V, Mione M, Carninci P, d'Adda di Fagagna F: Site-specific DICER and DROSHA RNA products control the DNA-damage response. *Nature* 488: 231–235, 2012
29. Knight SW, Bass BL: A role for the RNase III enzyme DCR-1 in RNA interference and germ line development in Caenorhabditis elegans. *Science* 293: 2269–2271, 2001
30. Ketting RF, Fischer SE, Bernstein E, Sijen T, Hannon GJ, Plasterk RH: Dicer functions in RNA interference and in synthesis of small RNA involved in developmental timing in C. elegans. *Genes Dev* 15: 2654–2659, 2001
31. Grishok A, Pasquinelli AE, Conte D, Li N, Parrish S, Ha I, Baillie DL, Fire A, Ruvkun G, Mello CC: Genes and mechanisms related to RNA interference regulate expression of the small temporal RNAs that control C. elegans developmental timing. *Cell* 106: 23–34, 2001
32. Ma M, Tian X, Igarashi P, Pazour GJ, Somlo S: Loss of cilia suppresses cyst growth in genetic models of autosomal dominant polycystic kidney disease. *Nat Genet* 45: 1004–1012, 2013
33. Patel V, Hajarnis S, Williams D, Hunter R, Huynh D, Igarashi P: MicroRNAs regulate renal tubule maturation through modulation of Pkd1. *J Am Soc Nephrol* 23: 1941–1948, 2012
34. Hajarnis S, Lakhia R, Yheskel M, Williams D, Sorourian M, Liu X, Aboudehen K, Zhang S, Kersjes K, Galasso R, Li J, Kaimal V, Lockton S, Davis S, Flaten A, Johnson JA, Holland WL, Kusminski CM, Scherer PE, Harris PC, Trudel M, Wallace DP, Igarashi P, Lee EC, Androsavich JR, Patel V: microRNA-17 family promotes polycystic kidney disease progression through modulation of mitochondrial metabolism. *Nat Commun* 8: 14395, 2017
35. Hajarnis S, Lakhia R, Patel V: MicroRNAs and polycystic kidney disease. In: *Polycystic Kidney Disease*, edited by Li X, Brisbane (AU), Codon Publications, 2015
36. Lakhia R, Hajarnis S, Williams D, Aboudehen K, Yheskel M, Xing C, Hatley ME, Torres VE, Wallace DP, Patel V: MicroRNA-21 aggravates cyst growth in a model of polycystic kidney disease. *J Am Soc Nephrol* 27: 2319–2330, 2016
37. Patel V, Williams D, Hajarnis S, Hunter R, Pontoglio M, Somlo S, Igarashi P: miR-17~92 miRNA cluster promotes kidney cyst growth in polycystic kidney disease. *Proc Natl Acad Sci U S A* 110: 10765–10770, 2013
38. Yheskel M, Patel V: Therapeutic microRNAs in polycystic kidney disease. *Curr Opin Nephrol Hypertens* 26: 282–289, 2017
39. Grande MT, Sánchez-Laorden B, López-Blau C, De Frutos CA, Boutet A, Arévalo M, Rowe RG, Weiss SJ, López-Novoa JM, Nieto MA: Snail1-induced partial epithelial-to-mesenchymal transition drives renal fibrosis in mice and can be targeted to reverse established disease. *Nat Med* 21: 989–997, 2015
40. Nieto MA, Huang RY, Jackson RA, Thiery JP: Emt: 2016. *Cell* 166: 21–45, 2016
41. Lovisa S, LeBleu VS, Tampe B, Sugimoto H, Vadnagara K, Carstens JL, Wu CC, Hagos Y, Burckhardt BC, Pentcheva-Hoang T, Nischal H, Allison JP, Zeisberg M, Kalluri R: Epithelial-to-mesenchymal transition induces cell cycle arrest and parenchymal damage in renal fibrosis. *Nat Med* 21: 998–1009, 2015
42. Ivanova L, Butt MJ, Matsell DG: Mesenchymal transition in kidney collecting duct epithelial cells. *Am J Physiol Renal Physiol* 294: F1238–F1248, 2008
43. Smith JP, Pozzi A, Dhawan P, Singh AB, Harris RC: Soluble HB-EGF induces epithelial-to-mesenchymal transition in inner medullary collecting duct cells by upregulating Snail-2. *Am J Physiol Renal Physiol* 296: F957–F965, 2009
44. Butt MJ, Tarantal AF, Jimenez DF, Matsell DG: Collecting duct epithelial-mesenchymal transition in fetal urinary tract obstruction. *Kidney Int* 72: 936–944, 2007
45. Gewin L, Bulus N, Mernaugh G, Moeckel G, Harris RC, Moses HL, Pozzi A, Zent R: TGF-beta receptor deletion in the renal collecting system exacerbates fibrosis. *J Am Soc Nephrol* 21: 1334–1343, 2010
46. Fujiu K, Manabe I, Nagai R: Renal collecting duct epithelial cells regulate inflammation in tubulointerstitial damage in mice. *J Clin Invest* 121: 3425–3441, 2011
47. Wang G, Kwan BC, Lai FM, Choi PC, Chow KM, Li PK, Szeto CC: Intrarenal expression of microRNAs in patients with IgA nephropathy. *Lab Invest* 90: 98–103, 2010
48. Ho JJ, Metcalf JL, Yan MS, Turgeon PJ, Wang JJ, Chalsev M, Petruzziello-Pellegrini TN, Tsui AK, He JZ, Dhamko H, Man HS, Robb GB, Teh BT, Ohh M, Marsden PA: Functional importance of Dicer protein in the adaptive cellular response to hypoxia. *J Biol Chem* 287: 29003–29020, 2012
49. Godwin JG, Ge X, Stephan K, Jurisch A, Tullius SG, Iacomini J: Identification of a microRNA signature of renal ischemia reperfusion injury. *Proc Natl Acad Sci U S A* 107: 14339–14344, 2010
50. Williams SS, Cobo-Stark P, Hajarnis S, Aboudehen K, Shao X, Richardson JA, Patel V, Igarashi P: Tissue-specific regulation of the mouse Pkhd1 (ARPKD) gene promoter. *Am J Physiol Renal Physiol* 307: F356–F368, 2014
51. Harfe BD, McManus MT, Mansfield JH, Hornstein E, Tabin CJ: The RNaseIII enzyme Dicer is required for morphogenesis but not patterning of the vertebrate limb. *Proc Natl Acad Sci U S A* 102: 10898–10903, 2005
52. Cheng CJ, Yoon J, Baum M, Huang CL: STE20/SPS1-related proline/alanine-rich kinase (SPAK) is critical for sodium reabsorption in isolated, perfused thick ascending limb. *Am J Physiol Renal Physiol* 308: F437–F443, 2015

See related editorial, "Insights into the Regulation of Collecting Duct Homeostasis by Small Noncoding RNAs," on pages 349–350.

This article contains supplemental material online at http://jasn.asnjournals.org/lookup/suppl/doi:10.1681/ASN.2017030334/-/DCSupplemental.

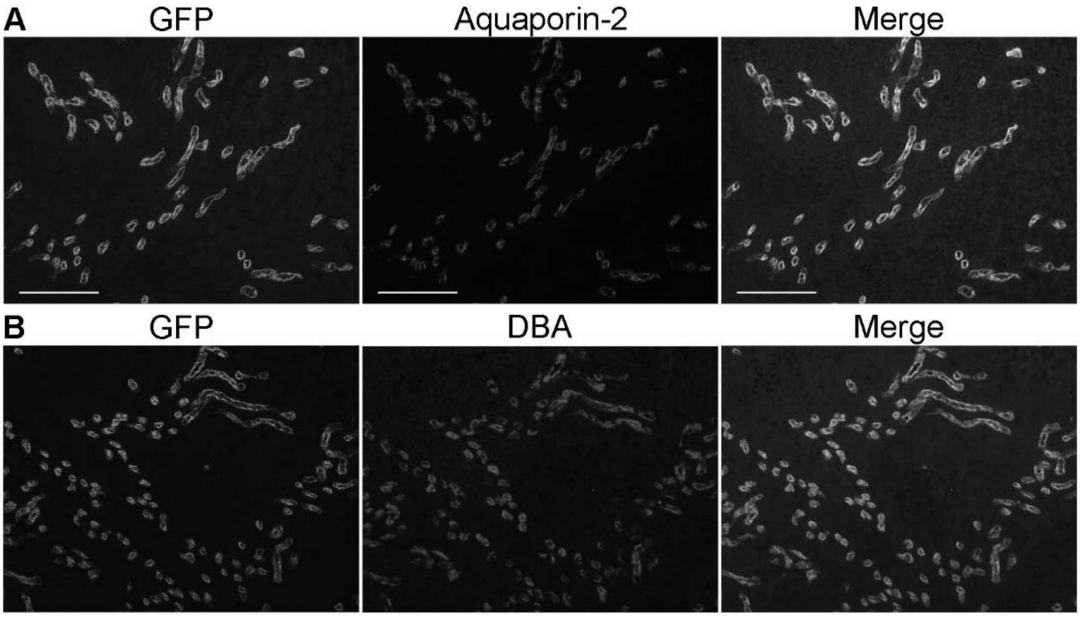

Supplementary Figure 1: Kidneys from 5-week-old Pkhd1/Cre; R26R-EYFP reporter mice were co-stained with GFP and collecting duct markers Aquaporin-2 **(A)** or DBA **(B).** Consistent with previous studies, we observed that a 100% of $EYFP^{+}$ tubules were also positive for Aquaporin-2 and DBA.

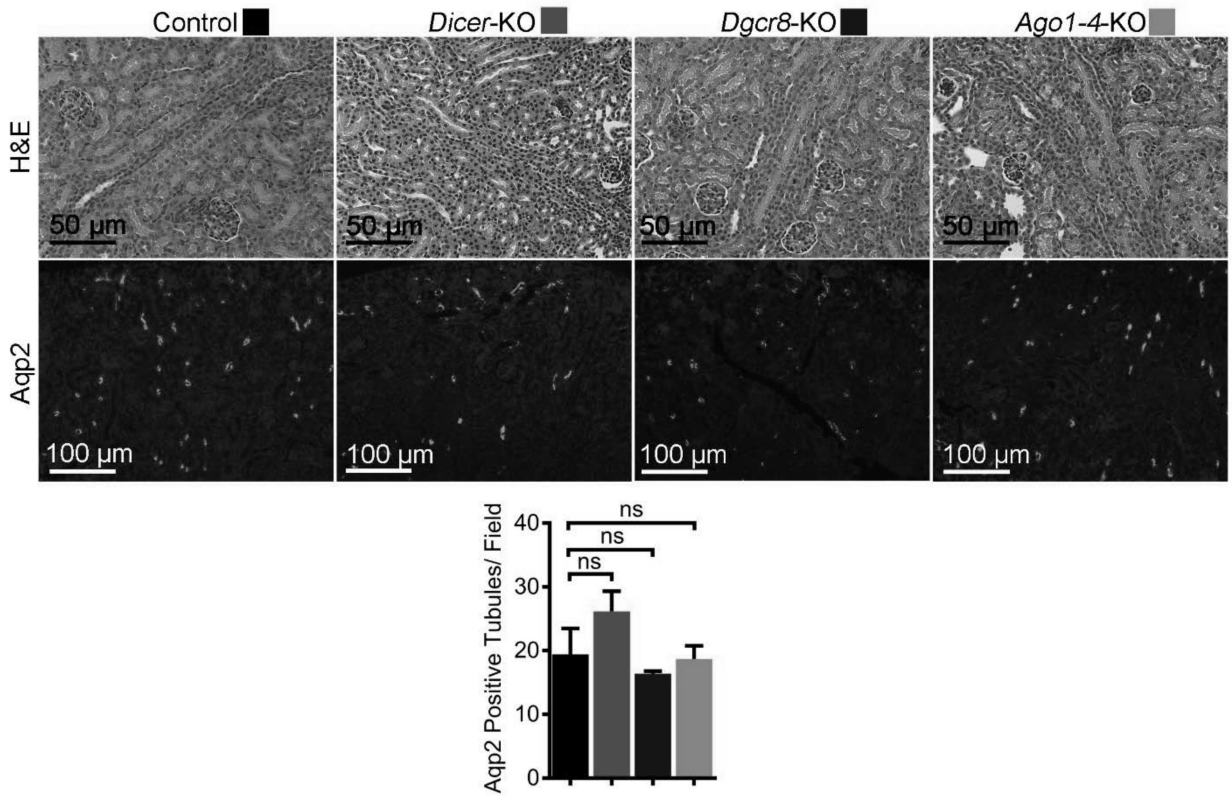

Supplementary Figure 2: *Dicer*-KO, *Dgcr8*-KO, and *Ago1-4*-KO mice exhibit normal kidney histology at P14. H&E staining of kidney sections from control, *Dicer*-KO, *Dgcr8*-KO, and *Ago1-4*-KO mice is shown (top panel). Anti-Aquaporin 2 staining showed an equal number of collecting ducts in kidneys of *Dicer*-KO, *Dgcr8*-KO, and *Ago1-4*-KO mice compared to control mice (middle panel). Quantification of number of Aquaporin-2 positive tubules shown (bottom panel). P indicates postnatal day. ns indicates $P>0.05$.

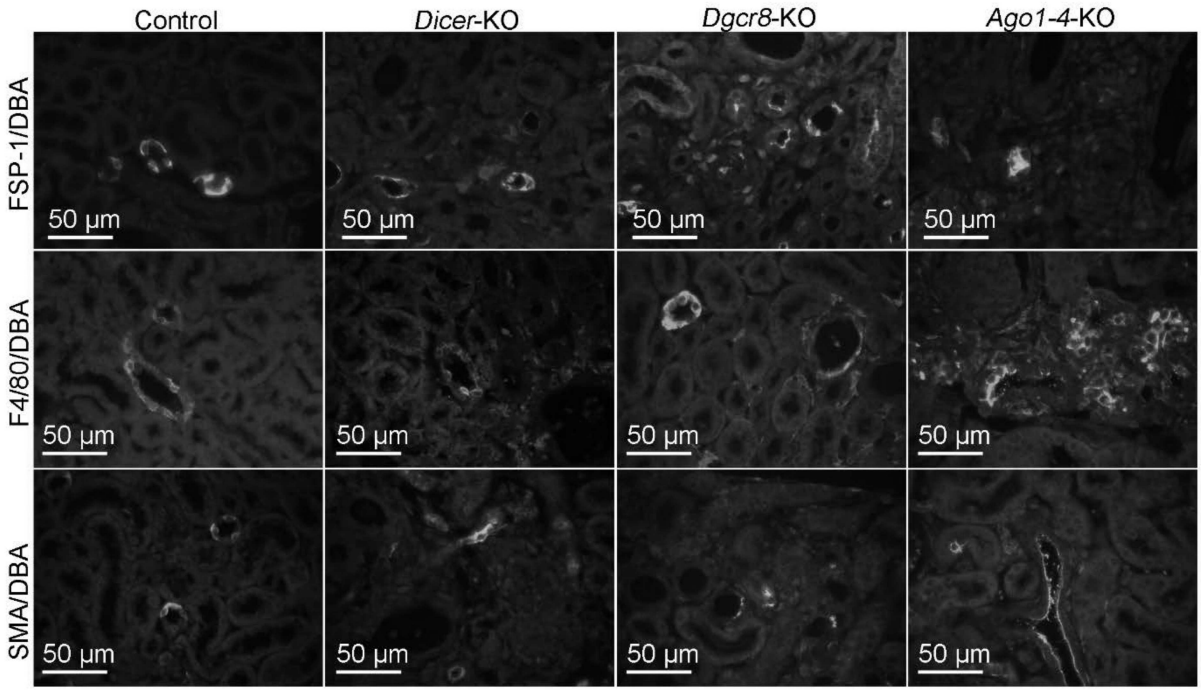

Supplementary Figure 3: Inflammatory infiltrates surround mutant collecting ducts. Kidneys from 5 week old control, Dicer-KO, Dgcr8-KO, and Ago1-4-KO mice were stained with antibodies against FSP-1, F4/80, and SMA. To determine the localization of these markers in reference to CDs, kidneys were co-stained with DBA.

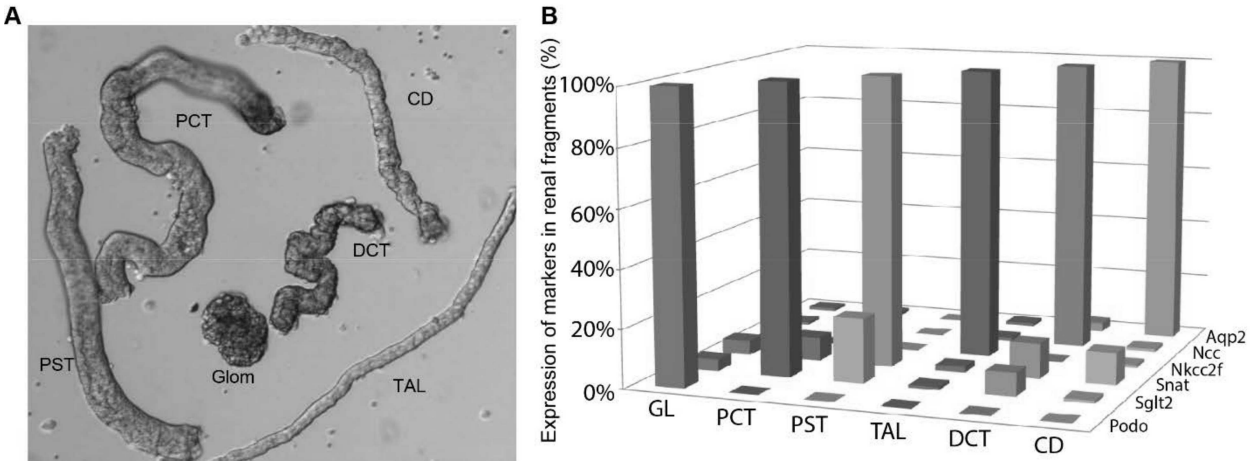

Supplementary Figure 4: Purity of microdissected nephron segments. (A) Representative phase contrast image of segments obtained after collagenase treatment of mouse kidneys. Microdissected segments: glomerulus (Glom); proximal convoluted tubules (PCT); proximal straight tubules (PST); thick ascending limbs (TAL); Distal convoluted tubule (DCT) and collecting ducts (CD). **(B)** Segment-specific marker genes (Glom: podocin; PT: *SGLT2* and *SNAT3*; TAL: *NKCC2* and *UMOD*; DCT: *NCC*; CDCD: *AQP2*) were used to demonstrate the purity for each fraction of collected tubule segments using SYBR green quantitative PCR. Quantification of all segment-specific marker genes was done in comparison with *GAPDH* as an endogenous control. Expression of segment-specific markers in the various renal fragments is shown.

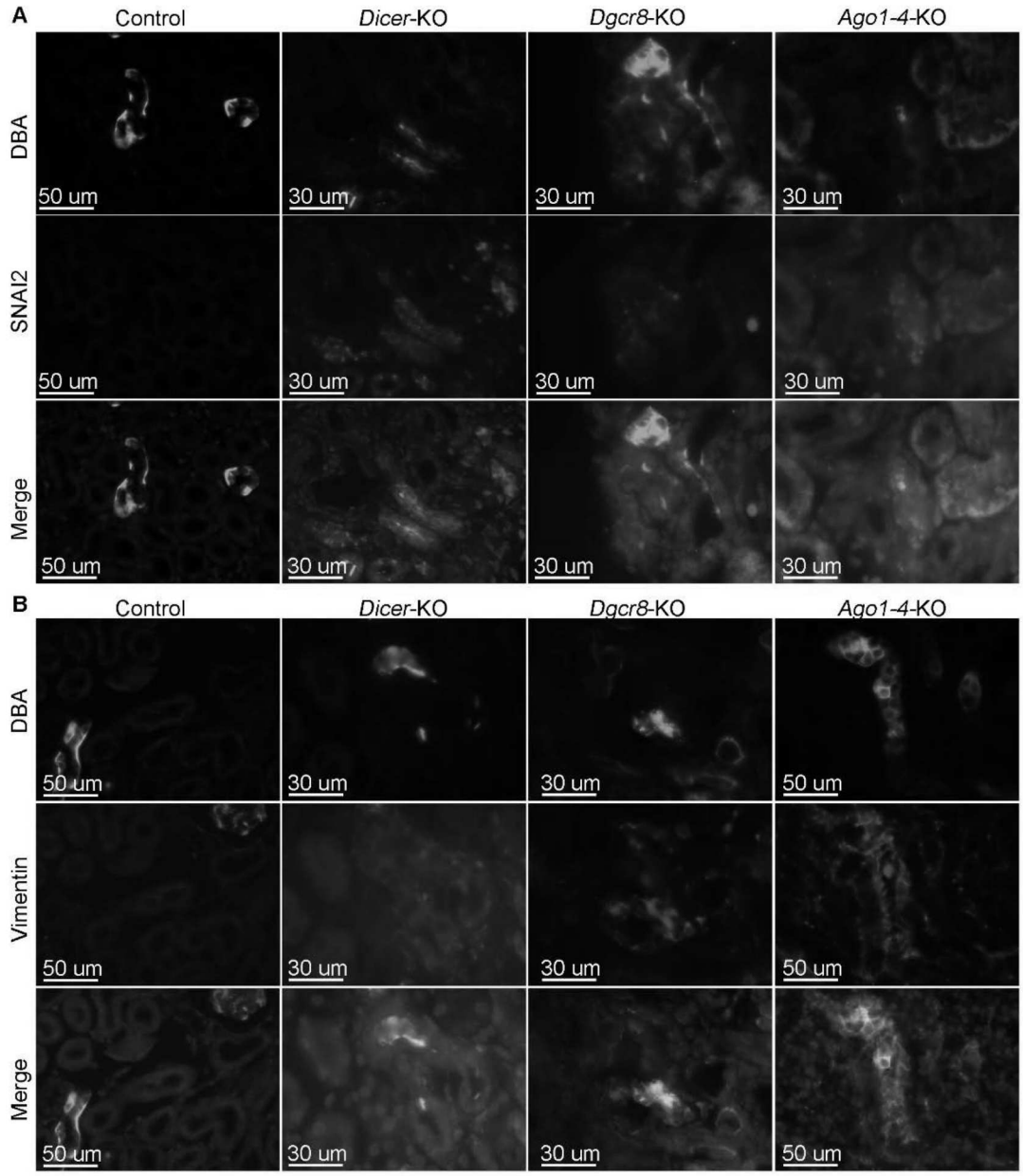

Supplementary Figure 5: Expression of mesenchymal markers SNAI2 and Vimentin in miRNA-depleted CDs. Immunohistochemistry staining of mesenchymal markers **(A)** SNAI2 and **(B)** Vimentin showed tubular co-localization with collecting duct-specific marker DBA of *Dicer*-KO, *Dgcr8*-KO, and *Ago1-4*-KO mice.

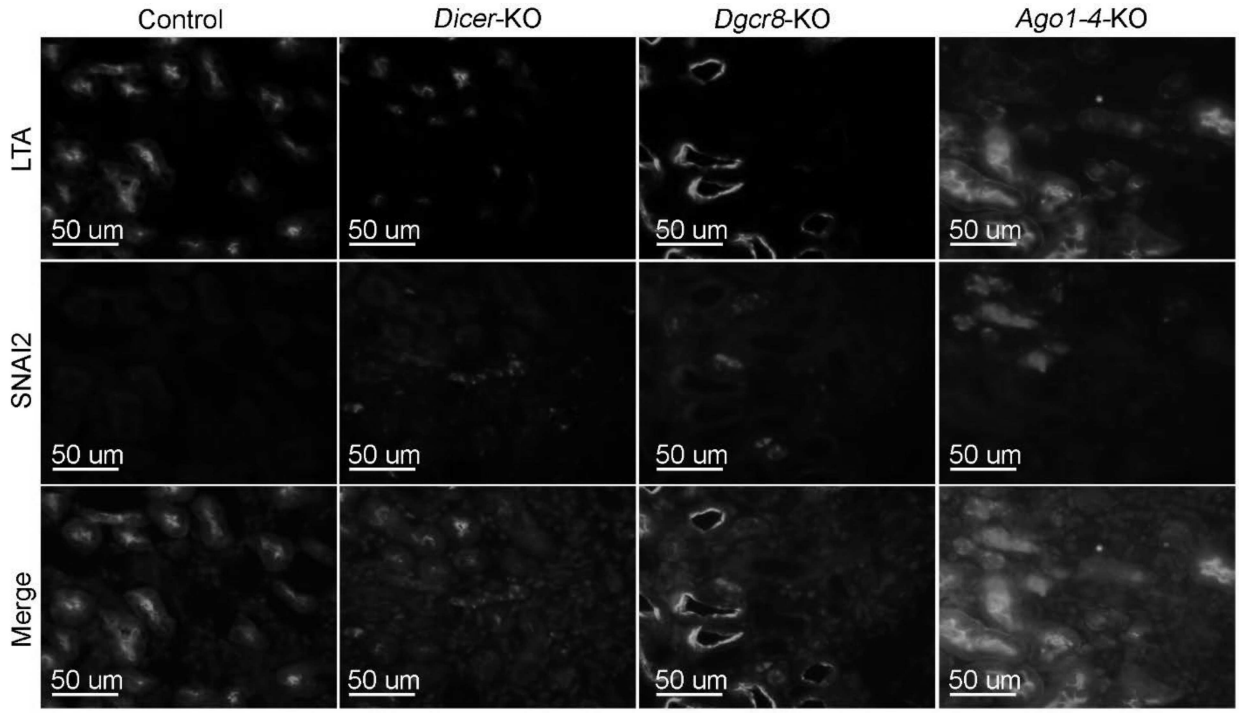

Supplementary Figure 6: Immunohistochemistry staining of mesenchymal marker SNAI2 showed no tubular co-localization with proximal tubule-specific marker LTA in kidneys of *Dicer*-KO, *Dgcr8*-KO, and *Ago1-4*-KO mice.

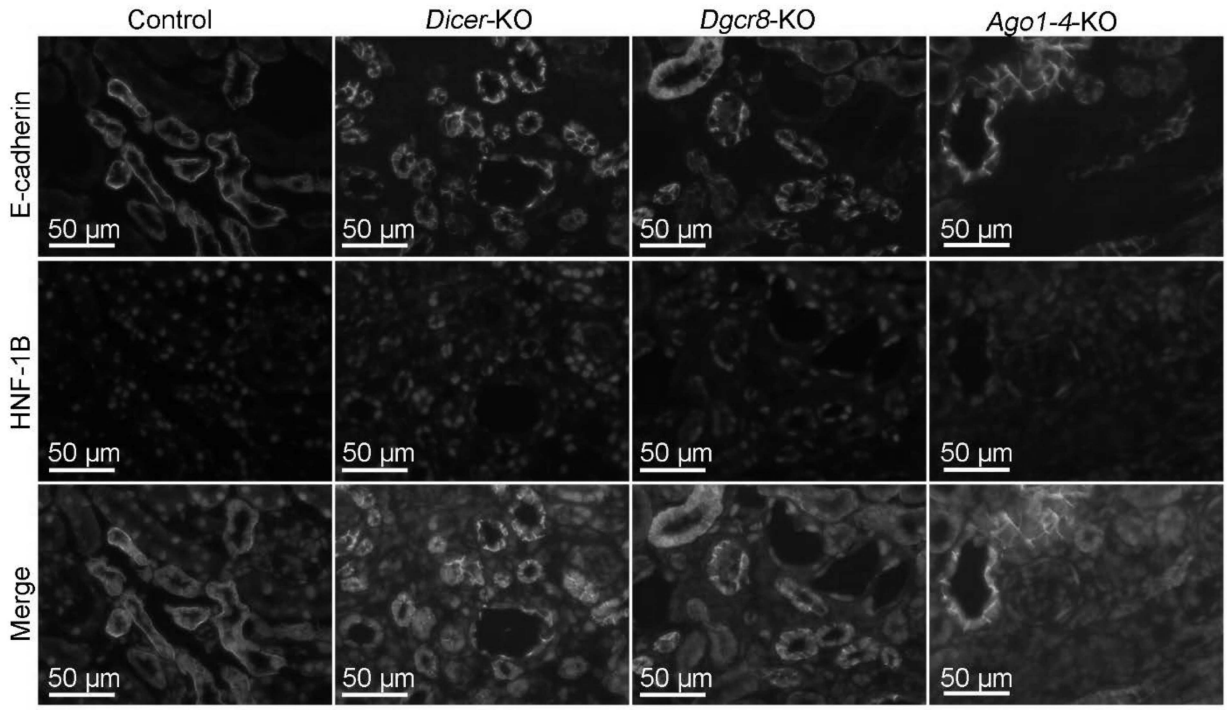

Supplementary Figure 7: Expression of epithelial markers E-cadherin and HNF-1β is unchanged in miRNA-mutant CDs. Immunohistochemistry staining of epithelial markers E-cadherin and HNF-1β showed normal expression in kidneys of *Dicer*-KO, *Dgcr8*-KO, and *Ago1-4*-KO mice compared to control mice at 5 weeks of age.

Supplementary Table 1: Segmental miRNA Expression Profile of Glomerulus, Nephron, and Collecting Duct

			Log2(Count)			
miRNA	mean GL	mean PCT	mean PST	mean TAL	mean DCT	mean CD
mmu-miR-200c-3p	3.62	2.63	2.28	7.79	7.58	8.74
mmu-miR-218-5p	4.99	2.81	2.47	7.46	7.19	7.02
mmu-miR-96-5p	2.10	2.20	2.90	2.23	2.55	6.28
mmu-miR-27a-3p	9.22	4.59	4.23	6.76	7.41	7.09
mmu-let-7i-5p	10.31	8.68	8.47	9.62	10.00	11.09
mmu-miR-23a-3p	10.79	6.46	6.13	8.51	8.83	8.67
mmu-miR-10a-5p	9.69	8.22	8.26	10.42	10.60	10.27
mmu-miR-23b-3p	11.54	7.65	7.36	9.20	9.66	9.37
mmu-miR-24-3p	11.74	8.29	8.14	9.74	10.21	9.95
mmu-miR-27b-3p	9.38	5.92	5.54	7.61	7.95	7.46
mmu-miR-20a-5p	7.07	6.63	7.22	7.59	6.75	7.97
mmu-miR-497-5p	8.69	4.65	4.56	6.16	6.43	5.89
mmu-miR-151-5p	8.31	6.41	6.40	7.85	8.56	7.41
mmu-miR-200a-3p	6.39	8.62	8.59	9.28	9.28	9.61
mmu-miR-195a-5p	9.05	5.07	5.03	6.63	6.68	5.93
mmu-let-7e-5p	9.74	8.69	7.20	9.51	9.45	9.48
mmu-miR-6368	5.38	6.15	6.01	6.32	6.60	6.72
mmu-miR-20b-5p	5.67	5.96	6.63	6.04	5.20	6.52
mmu-miR-200b-3p	6.07	9.20	9.46	9.31	9.48	9.64
mmu-miR-92a-3p	7.36	6.64	7.30	8.01	6.42	7.00
mmu-miR-429-3p	5.85	8.90	9.08	8.85	9.25	9.23
mmu-miR-125a-5p	7.39	6.37	4.82	6.85	6.75	6.53
mmu-miR-221-3p	4.57	7.16	6.83	6.72	6.94	7.30
mmu-miR-30e-5p	7.24	8.62	8.60	9.17	8.94	8.74
mmu-miR-451a	10.08	6.45	7.82	7.13	5.92	6.51
mmu-miR-5119	5.07	6.17	5.89	5.47	5.97	6.16
mmu-miR-26a-5p	10.81	9.42	9.60	9.38	9.04	9.39
mmu-miR-378d	5.83	7.15	7.34	8.70	7.73	7.08
mmu-miR-378a-3p	4.24	5.98	6.42	7.55	6.55	5.67
mmu-miR-378b	5.31	6.63	6.91	8.18	7.25	6.31
mmu-miR-126-3p	12.42	8.90	8.86	9.32	9.49	8.57
mmu-miR-5100	10.43	11.47	11.19	11.33	11.28	11.12
mmu-miR-5109	9.08	10.40	10.44	10.04	9.84	10.04
mmu-miR-130a-3p	9.94	8.88	8.66	8.53	8.48	8.42
mmu-miR-26b-5p	9.48	8.91	8.59	8.14	8.32	8.45
mmu-let-7a-5p	12.49	12.05	12.05	11.81	11.62	11.58
mmu-miR-98-5p	6.53	6.88	6.70	5.92	6.48	6.40
mmu-miR-22-3p	9.78	11.06	11.54	10.42	10.91	10.39
mmu-miR-21a-5p	8.15	10.38	10.62	7.78	8.92	9.70
mmu-miR-466i-5p	5.67	7.65	7.85	7.05	6.74	6.95
mmu-miR-196a-5p	7.92	7.91	7.64	8.25	7.84	7.18
mmu-miR-103-3p	7.89	8.24	8.59	7.18	7.69	7.49
mmu-miR-5126	8.22	9.78	9.64	9.67	9.39	9.02
mmu-miR-107-3p	8.21	9.23	10.17	8.72	8.64	8.44
mmu-miR-15a-5p	9.43	9.39	9.22	8.09	8.00	8.44
mmu-miR-3960	6.74	8.42	8.09	8.00	7.65	7.40
mmu-miR-16-5p	9.14	9.01	8.88	7.53	7.22	7.55
mmu-miR-34a-5p	6.94	7.87	8.90	6.68	7.96	6.33
mmu-miR-29c-3p	9.89	10.17	10.21	7.91	8.62	8.46

Supplementary Table 2: Microarray of Microdissected Collecting Ducts

miRNA	p-value	CTL Mean	St Dev	MUTANT Mean	St. Dev	Log2 (G2/G1)
mmu-miR-200c-3p	5.48E-03	549	28	119	24	-2.21
mmu-miR-3097-5p	7.21E-03	457	72	145	10	-1.65
mmu-miR-468-3p	3.90E-03	477	71	170	28	-1.49
mmu-let-7i-5p	3.83E-05	1,515	30	709	20	-1.10
mmu-miR-200a-3p	3.26E-04	1,020	8	508	10	-1.00
mmu-miR-451a	9.65E-03	2,938	120	1,590	150	-0.89
mmu-miR-10b-5p	2.49E-04	1,581	48	870	35	-0.86
mmu-miR-32-3p	5.13E-03	762	45	452	11	-0.75
mmu-miR-709	1.18E-03	23,454	1,099	14,548	697	-0.69
mmu-let-7j	8.21E-03	612	19	387	26	-0.66
mmu-miR-6348	1.50E-03	1,044	42	665	37	-0.65
mmu-miR-669c-5p	9.79E-03	1,198	84	773	18	-0.63
mmu-miR-429-3p	2.97E-03	526	30	350	20	-0.59
mmu-miR-30d-5p	6.40E-03	879	73	590	34	-0.58
mmu-let-7b-5p	1.04E-03	1,810	58	1,239	50	-0.55
mmu-miR-30b-5p	9.86E-03	2,197	137	1,528	6	-0.52
mmu-miR-130a-3p	6.39E-03	680	36	498	30	-0.45
mmu-miR-3082-5p	7.73E-03	1,636	72	1,204	85	-0.44
mmu-miR-574-5p	1.85E-03	2,252	67	1,809	37	-0.32
mmu-miR-3070b-3p	4.94E-03	414	21	533	16	0.37
mmu-miR-3963	7.23E-03	3,707	176	5,052	329	0.45
mmu-miR-133b-5p	6.66E-04	22,552	871	33,009	720	0.55
mmu-miR-145a-5p	5.61E-03	517	26	761	4	0.56
mmu-miR-5126	6.38E-03	1,221	93	1,834	126	0.59
mmu-miR-3068-3p	5.01E-03	336	18	533	9	0.66
mmu-miR-669c-3p	9.83E-03	1,025	174	2,063	212	1.01
mmu-miR-126-3p	4.01E-04	772	37	1,735	113	1.17
mmu-miR-706	2.49E-03	337	24	808	16	1.26
mmu-miR-669p-3p	5.83E-03	1,120	198	2,782	336	1.31
mmu-miR-669a-3p	1.87E-03	703	18	1,783	114	1.34
mmu-miR-574-3p	2.08E-03	515	37	1,309	29	1.34
mmu-miR-466h-3p	4.05E-04	1,361	104	3,473	180	1.35
mmu-miR-669f-3p	8.34E-03	605	123	1,592	243	1.40
mmu-miR-6240	6.96E-04	229	24	642	40	1.49
mmu-miR-466g	4.75E-04	537	49	1,547	99	1.53
mmu-miR-466i-3p	2.65E-04	875	5	2,550	75	1.54
mmu-miR-1903	4.15E-04	213	18	633	44	1.57
mmu-miR-466f-3p	1.69E-03	1,319	43	3,924	273	1.57
mmu-miR-6243	6.33E-04	1,066	22	3,260	143	1.61
mmu-miR-466m-3p	2.12E-03	512	43	1,583	57	1.63
mmu-miR-669e-3p	4.12E-03	465	83	1,444	219	1.63
mmu-miR-6239	2.72E-04	1,127	86	3,564	223	1.66
mmu-miR-5109	2.69E-04	594	53	1,981	103	1.74
mmu-miR-467a-3p	1.36E-03	207	34	821	93	1.99
mmu-miR-669a-3-3p	1.98E-04	130	11	569	44	2.13
mmu-miR-6538	4.10E-03	346	18	1,597	258	2.21
mmu-miR-467c-3p	1.27E-03	125	22	594	86	2.25
mmu-miR-6412	1.23E-04	130	9	1,133	139	3.12

Supplementary Table 3: Microdissected CD Full Data

miRNA	p-value	CTL Mean	St. Dev	MUTANT Mean	St. Dev2	Log2 (G2/G1)
mmu-let-7i-5p	3.83E-05	1,515	30	709	20	-1.10
mmu-miR-6412	1.23E-04	130	9	1,133	139	3.12
mmu-miR-669a-3-3p	1.98E-04	130	11	569	44	2.13
mmu-miR-10b-5p	2.49E-04	1,581	48	870	35	-0.86
mmu-miR-466i-3p	2.65E-04	875	5	2,550	75	1.54
mmu-miR-5109	2.69E-04	594	53	1,981	103	1.74
mmu-miR-6239	2.72E-04	1,127	86	3,564	223	1.66
mmu-miR-200a-3p	3.26E-04	1,020	8	508	10	-1.00
mmu-miR-126-3p	4.01E-04	772	37	1,735	113	1.17
mmu-miR-466h-3p	4.05E-04	1,361	104	3,473	180	1.35
mmu-miR-1903	4.15E-04	213	18	633	44	1.57
mmu-miR-466g	4.75E-04	537	49	1,547	99	1.53
mmu-miR-6243	6.33E-04	1,066	22	3,260	143	1.61
mmu-miR-133b-5p	6.66E-04	22,552	871	33,009	720	0.55
mmu-miR-6240	6.96E-04	229	24	642	40	1.49
mmu-let-7b-5p	1.04E-03	1,810	58	1,239	50	-0.55
mmu-miR-709	1.18E-03	23,454	1,099	14,548	697	-0.69
mmu-miR-467c-3p	1.27E-03	125	22	594	86	2.25
mmu-miR-467a-3p	1.36E-03	207	34	821	93	1.99
mmu-miR-6348	1.50E-03	1,044	42	665	37	-0.65
mmu-miR-466f-3p	1.69E-03	1,319	43	3,924	273	1.57
mmu-miR-574-5p	1.85E-03	2,252	67	1,809	37	-0.32
mmu-miR-669a-3p	1.87E-03	703	18	1,783	114	1.34
mmu-miR-574-3p	2.08E-03	515	37	1,309	29	1.34
mmu-miR-466m-3p	2.12E-03	512	43	1,583	57	1.63
mmu-miR-706	2.49E-03	337	24	808	16	1.26
mmu-miR-429-3p	2.97E-03	526	30	350	20	-0.59
mmu-miR-468-3p	3.90E-03	477	71	170	28	-1.49
mmu-miR-6538	4.10E-03	346	18	1,597	258	2.21
mmu-miR-669e-3p	4.12E-03	465	83	1,444	219	1.63
mmu-miR-3070b-3p	4.94E-03	414	21	533	16	0.37
mmu-miR-3068-3p	5.01E-03	336	18	533	9	0.66
mmu-miR-32-3p	5.13E-03	762	45	452	11	-0.75
mmu-miR-200c-3p	5.48E-03	549	28	119	24	-2.21
mmu-miR-145a-5p	5.61E-03	517	26	761	4	0.56
mmu-miR-669p-3p	5.83E-03	1,120	198	2,782	336	1.31
mmu-miR-5126	6.38E-03	1,221	93	1,834	126	0.59
mmu-miR-130a-3p	6.39E-03	680	36	498	30	-0.45
mmu-miR-30d-5p	6.40E-03	879	73	590	34	-0.58
mmu-miR-3097-5p	7.21E-03	457	72	145	10	-1.65
mmu-miR-3963	7.23E-03	3,707	176	5,052	329	0.45
mmu-miR-3082-5p	7.73E-03	1,636	72	1,204	85	-0.44
mmu-let-7j	8.21E-03	612	19	387	26	-0.66
mmu-miR-669f-3p	8.34E-03	605	123	1,592	243	1.40
mmu-miR-451a	9.65E-03	2,938	120	1,590	150	-0.89
mmu-miR-669c-5p	9.79E-03	1,198	84	773	18	-0.63

mmu-miR-669c-3p	9.83E-03	1,025	174	2,063	212	1.01
mmu-miR-30b-5p	9.86E-03	2,197	137	1,528	6	-0.52
mmu-miR-5129-5p	1.81E-05	48	3	0	0	-11.04
mmu-miR-196a-5p	2.21E-05	64	2	193	5	1.60
mmu-miR-199a-3p	3.39E-04	167	9	397	25	1.25
mmu-miR-297a-5p	4.61E-04	212	17	59	6	-1.85
mmu-miR-103-3p	4.72E-04	447	19	236	12	-0.92
mmu-miR-6368	5.68E-04	29	9	0	0	-10.25
mmu-miR-290-5p	9.00E-04	25	9	0	0	-10.00
mmu-miR-5110	1.24E-03	25	10	0	0	-9.99
mmu-miR-682	1.48E-03	25	10	0	0	-9.99
mmu-miR-223-3p	1.49E-03	0	0	72	45	14.23
mmu-let-7e-5p	1.68E-03	439	11	313	15	-0.49
mmu-miR-3084-5p	2.08E-03	0	0	100	69	14.64
mmu-miR-3084-3p	2.93E-03	126	14	272	28	1.11
mmu-miR-3085-3p	3.51E-03	46	8	126	15	1.45
mmu-miR-107-3p	3.72E-03	419	11	204	15	-1.04
mmu-miR-1839-3p	4.64E-03	16	4	74	19	2.23
mmu-miR-3099-3p	5.02E-03	317	26	186	18	-0.77
mmu-miR-804	5.14E-03	63	11	308	21	2.28
mmu-miR-328-5p	5.31E-03	71	13	30	3	-1.25
mmu-miR-194-1-3p	5.41E-03	0	0	107	94	14.72
mmu-miR-6345	5.62E-03	72	7	45	2	-0.67
mmu-miR-653-3p	5.93E-03	0	0	34	38	13.35
mmu-miR-1192	6.06E-03	183	23	338	27	0.88
mmu-miR-6349	6.74E-03	111	13	46	2	-1.26
mmu-miR-320-3p	6.80E-03	242	35	117	13	-1.04
mmu-miR-681	8.42E-03	91	7	33	5	-1.48
mmu-miR-1894-3p	9.55E-03	95	20	42	5	-1.17
mmu-miR-467b-3p	1.01E-02	779	136	2,414	185	1.63
mmu-miR-467d-3p	1.01E-02	543	98	1,732	141	1.67
mmu-miR-466q	1.04E-02	712	100	1,609	29	1.18
mmu-miR-568	1.04E-02	71	17	308	26	2.12
mmu-miR-122-5p	1.06E-02	626	39	90	29	-2.80
mmu-miR-30c-1-3p	1.09E-02	99	22	43	5	-1.21
mmu-miR-30c-5p	1.18E-02	4,444	159	3,654	40	-0.28
mmu-miR-3064-3p	1.22E-02	49	11	116	21	1.24
mmu-miR-192-5p	1.25E-02	215	24	410	22	0.93
mmu-miR-467f	1.26E-02	1,087	168	2,585	140	1.25
mmu-miR-5113	1.33E-02	298	39	159	24	-0.90
mmu-miR-3074-2-3p	1.34E-02	24	6	62	12	1.35
mmu-miR-5117-5p	1.37E-02	165	41	520	12	1.66
mmu-let-7g-5p	1.37E-02	783	31	964	55	0.30
mmu-miR-762	1.43E-02	789	50	1,537	189	0.96
mmu-miR-1966-5p	1.47E-02	253	16	181	4	-0.48
mmu-miR-1187	1.49E-02	1,258	22	975	50	-0.37
mmu-miR-5119	1.52E-02	286	49	127	26	-1.16
mmu-miR-219-2-3p	1.55E-02	3	1	45	26	3.80
mmu-miR-29a-3p	1.57E-02	210	10	129	13	-0.70

mmu-miR-30a-5p	1.67E-02	1,635	91	1,279	87	-0.36
mmu-miR-130b-3p	1.67E-02	18	6	84	31	2.18
mmu-miR-669f-5p	1.72E-02	917	85	578	78	-0.66
mmu-miR-6540-5p	1.72E-02	52	12	142	37	1.45
mmu-miR-3471	1.73E-02	0	0	90	86	14.49
mmu-miR-5624-5p	1.76E-02	34	8	98	30	1.54
mmu-let-7k	1.87E-02	338	26	268	11	-0.33
mmu-miR-3095-3p	1.88E-02	594	98	337	41	-0.82
mmu-miR-125b-5p	1.93E-02	423	19	517	32	0.29
mmu-miR-5105	1.96E-02	196	31	392	25	1.00
mmu-miR-200b-3p	1.99E-02	706	29	605	25	-0.22
mmu-miR-467e-3p	2.08E-02	80	31	481	60	2.59
mmu-miR-3472	2.12E-02	14	9	82	35	2.57
mmu-miR-214-3p	2.15E-02	343	40	481	31	0.49
mmu-miR-26b-5p	2.17E-02	386	13	650	82	0.75
mmu-miR-466b-5p	2.18E-02	214	20	90	17	-1.25
mmu-miR-1224-3p	2.19E-02	18	11	155	21	3.07
mmu-miR-466f	2.36E-02	476	14	248	42	-0.94
mmu-miR-16-5p	2.41E-02	1,498	37	1,175	72	-0.35
mmu-miR-466j	2.44E-02	243	2	134	22	-0.86
mmu-let-7f-5p	2.50E-02	1,760	37	2,175	118	0.31
mmu-miR-503-5p	2.53E-02	76	17	36	7	-1.07
mmu-miR-466f-5p	2.53E-02	542	12	372	38	-0.54
mmu-miR-466m-5p	2.54E-02	919	29	583	71	-0.66
mmu-miR-466d-3p	2.54E-02	20	10	164	23	3.03
mmu-miR-219-5p	2.63E-02	71	22	222	11	1.65
mmu-miR-5106	2.68E-02	89	17	34	13	-1.38
mmu-miR-652-3p	2.70E-02	62	11	120	9	0.95
mmu-miR-669l-5p	2.73E-02	509	98	257	50	-0.99
mmu-miR-485-3p	2.74E-02	887	146	1,578	22	0.83
mmu-miR-672-5p	2.95E-02	127	37	47	5	-1.45
mmu-miR-6539	2.96E-02	6	5	83	18	3.77
mmu-let-7c-5p	2.99E-02	3,112	34	2,631	134	-0.24
mmu-miR-3473e	3.00E-02	35	14	166	29	2.26
mmu-miR-1966-3p	3.12E-02	49	10	86	11	0.81
mmu-miR-344f-3p	3.14E-02	17	5	57	26	1.72
mmu-miR-669o-5p	3.19E-02	482	97	203	64	-1.24
mmu-miR-3098-3p	3.20E-02	148	10	75	15	-0.98
mmu-miR-143-3p	3.22E-02	291	52	514	31	0.82
mmu-miR-466c-5p	3.27E-02	758	39	481	64	-0.66
mmu-miR-3099-5p	3.32E-02	82	13	135	4	0.72
mmu-miR-703	3.32E-02	37	4	88	23	1.25
mmu-miR-17-5p	3.32E-02	191	6	153	10	-0.31
mmu-miR-669n	3.35E-02	1,295	208	850	76	-0.61
mmu-miR-21a-5p	3.43E-02	784	39	660	42	-0.25
mmu-miR-705	3.52E-02	238	14	194	15	-0.29
mmu-miR-3475	3.60E-02	0	0	84	25	8.97
mmu-miR-10a-5p	3.64E-02	930	30	676	70	-0.46
mmu-miR-494-3p	3.75E-02	105	53	401	44	1.93

mmu-miR-652-5p	3.76E-02	162	35	83	18	-0.97
mmu-miR-669b-5p	3.85E-02	308	14	129	43	-1.26
mmu-miR-1928	3.89E-02	23	8	69	28	1.57
mmu-miR-5121	3.93E-02	125	32	274	35	1.13
mmu-miR-615-3p	3.94E-02	95	22	50	2	-0.94
mmu-let-7d-3p	4.05E-02	211	19	83	25	-1.35
mmu-miR-873b	4.07E-02	7	4	46	28	2.67
mmu-miR-20a-5p	4.09E-02	189	12	157	4	-0.27
mmu-miR-30c-2-3p	4.16E-02	112	8	48	16	-1.21
mmu-miR-21a-3p	4.18E-02	33	14	84	21	1.37
mmu-miR-5107-5p	4.20E-02	266	15	177	24	-0.59
mmu-miR-3076-5p	4.24E-02	40	15	86	15	1.09
mmu-miR-1929-3p	4.27E-02	22	9	63	24	1.49
mmu-miR-5100	4.32E-02	2,299	68	2,780	174	0.27
mmu-miR-5099	4.33E-02	633	28	824	71	0.38
mmu-miR-466a-5p	4.40E-02	169	30	82	28	-1.04
mmu-miR-301a-3p	4.50E-02	117	7	66	13	-0.82
mmu-miR-6385	4.59E-02	201	17	123	22	-0.70
mmu-miR-6351	4.69E-02	74	22	35	7	-1.07
mmu-miR-19b-3p	4.74E-02	212	21	278	9	0.39
mmu-miR-5623-5p	4.75E-02	25	14	86	34	1.78
mmu-miR-383-3p	4.75E-02	117	11	70	13	-0.74
mmu-miR-669k-5p	4.81E-02	386	72	113	47	-1.78
mmu-miR-344c-5p	4.84E-02	52	16	103	23	0.97
mmu-miR-541-3p	4.94E-02	36	20	152	38	2.08
mmu-miR-874-3p	5.04E-02	55	6	115	31	1.07
mmu-miR-1195	5.22E-02	376	19	440	30	0.22
mmu-miR-423-5p	5.24E-02	167	8	63	25	-1.41
mmu-miR-5097	5.28E-02	234	14	342	48	0.55
mmu-miR-3473b	5.28E-02	71	31	243	7	1.77
mmu-miR-222-5p	5.29E-02	1	1	126	30	7.88
mmu-miR-223-5p	5.30E-02	0	1	90	89	7.60
mmu-miR-483-5p	5.31E-02	600	123	388	45	-0.63
mmu-miR-1931	5.45E-02	41	17	99	3	1.28
mmu-miR-1941-5p	5.47E-02	14	9	93	25	2.74
mmu-miR-378d	5.52E-02	148	18	114	10	-0.38
mmu-miR-151-5p	5.56E-02	171	8	199	15	0.22
mmu-miR-375-3p	5.65E-02	97	3	34	18	-1.53
mmu-miR-342-3p	5.71E-02	61	8	44	2	-0.47
mmu-miR-6366	5.74E-02	94	9	21	11	-2.18
mmu-miR-758-5p	5.76E-02	77	21	149	17	0.96
mmu-miR-1932	5.77E-02	38	14	106	19	1.47
mmu-miR-322-5p	5.80E-02	60	32	177	21	1.56
mmu-miR-3473a	5.80E-02	35	19	112	51	1.69
mmu-miR-129-5p	5.93E-02	84	18	149	35	0.83
mmu-miR-5112	6.01E-02	225	36	156	6	-0.53
mmu-miR-6417	6.03E-02	35	16	95	7	1.45
mmu-miR-3073b-3p	6.31E-02	10	5	36	17	1.90
mmu-miR-3960	6.41E-02	1,228	30	1,461	108	0.25

mmu-miR-218-5p	6.42E-02	100	32	188	8	0.91
mmu-miR-6416-3p	6.45E-02	37	24	121	18	1.72
mmu-miR-6360	6.66E-02	212	47	131	26	-0.70
mmu-miR-1843b-5p	6.67E-02	57	15	24	9	-1.26
mmu-miR-149-3p	6.69E-02	1,402	70	1,206	96	-0.22
mmu-miR-467g	6.75E-02	132	67	479	48	1.86
mmu-miR-3086-3p	6.95E-02	1	2	113	39	6.78
mmu-miR-3082-3p	6.95E-02	29	10	70	13	1.27
mmu-miR-1897-5p	6.98E-02	79	10	54	11	-0.54
mmu-miR-297b-5p	7.02E-02	116	15	42	18	-1.46
mmu-miR-1929-5p	7.61E-02	26	12	62	21	1.24
mmu-miR-374c-3p	7.62E-02	30	14	1	2	-4.98
mmu-miR-3470b	7.62E-02	27	16	110	31	2.00
mmu-miR-466a-3p	7.92E-02	2	4	183	30	6.36
mmu-miR-1895	7.95E-02	268	31	203	30	-0.41
mmu-miR-3085-5p	8.06E-02	21	13	91	30	2.12
mmu-miR-1912-5p	8.08E-02	16	7	34	5	1.05
mmu-miR-466k	8.15E-02	28	15	71	24	1.33
mmu-miR-674-5p	8.56E-02	85	35	31	17	-1.44
mmu-miR-3107-5p	8.94E-02	128	8	57	30	-1.16
mmu-miR-3078-5p	8.95E-02	24	8	64	36	1.45
mmu-miR-378a-5p	9.02E-02	85	24	43	15	-1.00
mmu-miR-344h-3p	9.02E-02	1	1	30	34	5.89
mmu-miR-6241	9.09E-02	118	20	84	14	-0.48
mmu-miR-341-5p	9.27E-02	56,375	3,722	49,552	3,070	-0.19
mmu-miR-3470a	9.28E-02	28	11	73	31	1.35
mmu-miR-466n-5p	9.34E-02	176	75	86	22	-1.03
mmu-miR-3083-5p	9.35E-02	2	4	89	35	5.41
mmu-miR-1940	9.36E-02	2	4	115	73	5.81
mmu-miR-222-3p	9.52E-02	121	15	151	8	0.32
mmu-miR-598-5p	9.54E-02	88	28	45	19	-0.96
mmu-miR-221-5p	9.59E-02	0	0	18	19	12.46
mmu-miR-6537-5p	9.72E-02	2	3	85	18	5.47
mmu-miR-344g-5p	9.85E-02	83	16	129	32	0.64
mmu-miR-3102-5p	1.01E-01	146	19	110	18	-0.40
mmu-let-7d-5p	1.01E-01	1,646	10	1,731	51	0.07
mmu-miR-3086-5p	1.01E-01	2	2	94	30	5.75
mmu-miR-1936	1.01E-01	7	5	52	38	2.91
mmu-miR-3081-5p	1.03E-01	19	17	76	19	2.01
mmu-miR-1264-3p	1.04E-01	0	0	47	80	14.17
mmu-let-7f-2-3p	1.05E-01	46	22	2	3	-4.67
mmu-miR-3473d	1.07E-01	9	8	71	42	2.94
mmu-miR-26a-5p	1.08E-01	2,496	116	2,795	195	0.16
mmu-miR-3081-3p	1.08E-01	12	14	75	25	2.61
mmu-miR-873a-3p	1.09E-01	4	7	122	83	4.98
mmu-miR-3572-5p	1.09E-01	0	0	44	44	13.58
mmu-miR-871-5p	1.09E-01	6	10	164	57	4.80
mmu-miR-466b-3p	1.09E-01	14	12	97	32	2.82
mmu-miR-6420	1.10E-01	0	0	42	37	13.46

mmu-miR-5615-3p	1.10E-01	3	4	68	39	4.75
mmu-miR-721	1.11E-01	155	31	45	28	-1.77
mmu-miR-130b-5p	1.12E-01	0	0	50	43	13.67
mmu-miR-704	1.14E-01	30	8	3	4	-3.57
mmu-miR-130a-5p	1.14E-01	0	0	66	64	14.09
mmu-miR-5619-5p	1.15E-01	0	0	81	93	14.40
mmu-miR-22-3p	1.15E-01	500	105	352	29	-0.50
mmu-miR-99b-5p	1.15E-01	325	73	214	26	-0.60
mmu-miR-3094-3p	1.16E-01	0	0	64	56	14.00
mmu-miR-296-5p	1.16E-01	93	20	65	11	-0.51
mmu-miR-374c-5p	1.16E-01	30	7	3	5	-3.49
mmu-miR-130c	1.16E-01	0	0	68	59	14.06
mmu-miR-1247-3p	1.16E-01	11	2	31	18	1.49
mmu-miR-1938	1.17E-01	4	7	78	29	4.26
mmu-miR-27b-3p	1.17E-01	628	74	521	47	-0.27
mmu-miR-3087-3p	1.17E-01	0	0	77	68	14.25
mmu-miR-190b-5p	1.19E-01	0	0	12	20	12.71
mmu-miR-191-5p	1.21E-01	396	40	464	19	0.23
mmu-miR-1843b-3p	1.21E-01	3	6	49	6	3.91
mmu-miR-5618-3p	1.21E-01	7	12	127	49	4.19
mmu-miR-106a-5p	1.21E-01	92	19	66	11	-0.49
mmu-miR-3094-5p	1.22E-01	0	0	116	101	14.77
mmu-miR-375-5p	1.23E-01	125	16	51	27	-1.28
mmu-miR-30e-5p	1.23E-01	1,292	80	1,169	31	-0.14
mmu-miR-5620-3p	1.23E-01	0	0	14	25	13.00
mmu-miR-1251-3p	1.25E-01	70	20	118	36	0.76
mmu-miR-3100-5p	1.25E-01	72	15	24	15	-1.60
mmu-miR-3079-3p	1.27E-01	7	9	29	11	1.96
mmu-miR-490-3p	1.27E-01	66	32	25	17	-1.42
mmu-miR-34b-3p	1.28E-01	3	5	53	46	4.19
mmu-miR-465a-5p	1.30E-01	0	0	21	37	13.58
mmu-miR-2136	1.31E-01	0	0	22	38	13.62
mmu-miR-1306-5p	1.31E-01	41	28	154	47	1.90
mmu-miR-5625-5p	1.31E-01	4	7	67	44	3.95
mmu-miR-671-5p	1.32E-01	90	23	40	18	-1.18
mmu-miR-465b-5p	1.33E-01	0	0	24	42	13.77
mmu-miR-5617-5p	1.34E-01	25	31	100	39	2.03
mmu-miR-346-3p	1.36E-01	122	18	169	39	0.46
mmu-miR-1264-5p	1.36E-01	0	0	29	51	14.04
mmu-miR-5616-3p	1.36E-01	3	6	54	34	3.95
mmu-miR-669a-5p	1.37E-01	314	14	114	77	-1.46
mmu-miR-802-5p	1.39E-01	0	0	34	59	14.26
mmu-miR-191-3p	1.40E-01	26	3	40	10	0.63
mmu-miR-5617-3p	1.41E-01	52	32	113	43	1.11
mmu-miR-6340	1.42E-01	53	17	13	14	-1.98
mmu-miR-376a-3p	1.42E-01	77	21	24	18	-1.66
mmu-miR-551b-5p	1.43E-01	2	2	50	7	4.57
mmu-miR-219-1-3p	1.43E-01	46	28	102	15	1.16
mmu-miR-34a-5p	1.44E-01	18	13	39	4	1.14

mmu-miR-466e-5p	1.44E-01	145	16	105	24	-0.46
mmu-let-7b-3p	1.44E-01	72	7	33	25	-1.13
mmu-miR-344e-5p	1.44E-01	0	0	36	43	8.70
mmu-miR-1962	1.45E-01	126	17	65	38	-0.96
mmu-miR-5103	1.45E-01	30	12	5	8	-2.74
mmu-miR-3572-3p	1.46E-01	0	0	52	91	14.87
mmu-miR-1981-5p	1.47E-01	33	9	50	13	0.63
mmu-miR-675-5p	1.48E-01	70	48	27	10	-1.39
mmu-miR-181a-5p	1.49E-01	720	28	819	73	0.19
mmu-miR-3088-5p	1.49E-01	0	0	64	111	15.16
mmu-miR-541-5p	1.50E-01	11	12	50	32	2.23
mmu-miR-1906	1.51E-01	57	17	81	3	0.50
mmu-miR-1905	1.55E-01	22	10	46	12	1.07
mmu-miR-3102-3p.2-3p	1.58E-01	66	8	26	27	-1.34
mmu-miR-6370	1.59E-01	60	11	9	15	-2.76
mmu-miR-344i	1.60E-01	65	23	115	45	0.83
mmu-miR-6406	1.61E-01	30	18	12	6	-1.35
mmu-miR-196b-3p	1.61E-01	74	13	90	8	0.29
mmu-miR-677-3p	1.62E-01	85	29	126	12	0.56
mmu-miR-6419	1.62E-01	5	6	81	27	4.09
mmu-miR-5626-3p	1.64E-01	7	12	79	62	3.50
mmu-miR-34c-3p	1.64E-01	141	60	260	49	0.88
mmu-miR-5624-3p	1.64E-01	0	0	71	86	10.99
mmu-miR-6359	1.65E-01	64	20	13	12	-2.34
mmu-miR-501-3p	1.65E-01	25	11	5	9	-2.22
mmu-miR-654-5p	1.65E-01	33	20	65	23	0.97
mmu-miR-409-3p	1.66E-01	116	31	73	25	-0.66
mmu-miR-1930-5p	1.66E-01	6	10	52	9	3.09
mmu-miR-291a-5p	1.66E-01	84	23	34	31	-1.30
mmu-miR-363-5p	1.68E-01	1,175	85	1,016	123	-0.21
mmu-miR-132-3p	1.69E-01	5	6	86	56	4.25
mmu-miR-335-5p	1.71E-01	2	4	23	25	3.26
mmu-miR-466p-5p	1.72E-01	199	10	97	52	-1.03
mmu-miR-382-3p	1.72E-01	51	21	17	12	-1.55
mmu-miR-7b-3p	1.73E-01	48	39	100	18	1.07
mmu-miR-1952	1.74E-01	106	35	41	29	-1.36
mmu-miR-28a-5p	1.75E-01	63	42	17	11	-1.91
mmu-miR-714	1.76E-01	53	21	80	6	0.61
mmu-miR-6236	1.77E-01	200	35	159	13	-0.33
mmu-miR-615-5p	1.79E-01	339	52	283	25	-0.26
mmu-miR-3093-5p	1.79E-01	41	10	118	69	1.52
mmu-miR-3105-5p	1.80E-01	85	13	43	25	-0.97
mmu-miR-1941-3p	1.81E-01	4	4	58	19	3.89
mmu-miR-103-2-5p	1.82E-01	24	12	48	11	0.98
mmu-miR-1196-5p	1.85E-01	92	19	133	37	0.53
mmu-miR-3083-3p	1.86E-01	0	0	34	32	7.01
mmu-miR-770-5p	1.87E-01	38	21	74	13	0.98
mmu-miR-350-5p	1.87E-01	41	31	83	23	1.01
mmu-miR-351-3p	1.88E-01	66	30	105	17	0.68

mmu-miR-3104-3p	1.90E-01	118	15	72	37	-0.71
mmu-miR-21c	1.90E-01	0	0	28	32	6.62
mmu-miR-101a-3p	1.91E-01	39	19	76	22	0.95
mmu-miR-297c-5p	1.92E-01	85	5	32	31	-1.43
mmu-miR-98-3p	1.97E-01	95	28	9	12	-3.36
mmu-miR-653-5p	1.97E-01	6	10	44	10	2.84
mmu-miR-378c	1.98E-01	200	24	171	19	-0.23
mmu-miR-125a-5p	1.99E-01	243	3	217	22	-0.16
mmu-miR-351-5p	1.99E-01	50	37	96	21	0.93
mmu-miR-128-2-5p	2.00E-01	5	4	71	50	3.98
mmu-miR-3961	2.04E-01	105	15	64	29	-0.71
mmu-miR-106b-5p	2.04E-01	114	15	73	27	-0.63
mmu-miR-148a-3p	2.05E-01	117	14	88	24	-0.42
mmu-miR-668-5p	2.06E-01	45	31	86	31	0.92
mmu-miR-195a-5p	2.09E-01	268	54	328	20	0.29
mmu-miR-290-3p	2.09E-01	66	30	32	24	-1.03
mmu-miR-6394	2.10E-01	45	7	19	22	-1.24
mmu-miR-1933-3p	2.10E-01	6	9	59	35	3.21
mmu-miR-148b-3p	2.10E-01	108	29	75	17	-0.52
mmu-miR-3074-1-3p	2.11E-01	25	14	57	27	1.20
mmu-miR-379-5p	2.12E-01	63	12	26	18	-1.25
mmu-miR-6352	2.13E-01	90	10	9	8	-3.30
mmu-miR-196a-1-3p	2.13E-01	65	31	103	9	0.67
mmu-miR-675-3p	2.13E-01	83	2	50	25	-0.75
mmu-miR-25-5p	2.13E-01	24	40	109	59	2.20
mmu-miR-1933-5p	2.14E-01	0	0	47	81	10.07
mmu-miR-376c-3p	2.20E-01	20	3	11	20	-0.78
mmu-miR-6541	2.23E-01	15	14	66	7	2.10
mmu-miR-871-3p	2.23E-01	7	6	65	10	3.18
mmu-miR-1298-3p	2.23E-01	16	14	50	33	1.65
mmu-miR-10a-3p	2.24E-01	47	10	6	5	-2.96
mmu-miR-126-5p	2.24E-01	0	0	49	84	9.83
mmu-miR-491-5p	2.24E-01	27	5	17	30	-0.64
mmu-miR-760-5p	2.25E-01	41	3	54	12	0.39
mmu-miR-29b-3p	2.26E-01	22	5	14	24	-0.65
mmu-miR-1955-3p	2.26E-01	119	19	59	44	-1.00
mmu-miR-380-5p	2.27E-01	45	20	13	23	-1.73
mmu-miR-670-5p	2.29E-01	100	27	12	11	-3.11
mmu-miR-3544-3p	2.30E-01	42	34	83	36	0.98
mmu-miR-690	2.30E-01	11,161	247	11,840	640	0.09
mmu-miR-1251-5p	2.32E-01	30	19	59	26	0.96
mmu-miR-5619-3p	2.32E-01	1	2	85	90	6.51
mmu-miR-6343	2.33E-01	39	22	5	5	-2.89
mmu-miR-673-5p	2.34E-01	24	10	17	29	-0.55
mmu-miR-23a-3p	2.34E-01	1,254	136	1,392	82	0.15
mmu-miR-127-5p	2.35E-01	21	9	72	47	1.75
mmu-miR-700-3p	2.35E-01	74	19	102	28	0.46
mmu-miR-6244	2.35E-01	30	8	22	39	-0.40
mmu-miR-5108	2.37E-01	65	14	9	9	-2.82

mmu-miR-341-3p	2.38E-01	236	17	289	53	0.29
mmu-miR-466l-3p	2.38E-01	1	2	98	85	6.53
mmu-miR-381-3p	2.39E-01	59	21	8	7	-2.86
mmu-miR-873a-5p	2.42E-01	12	15	86	42	2.81
mmu-miR-379-3p	2.44E-01	35	5	9	14	-1.92
mmu-miR-1935	2.44E-01	42	14	75	33	0.84
mmu-miR-6354	2.46E-01	47	2	13	20	-1.87
mmu-miR-344b-5p	2.46E-01	1	2	41	40	5.33
mmu-miR-214-5p	2.46E-01	16	9	43	30	1.41
mmu-miR-6337	2.47E-01	71	13	40	23	-0.82
mmu-miR-3102-3p	2.47E-01	51	9	8	7	-2.65
mmu-miR-496a-5p	2.48E-01	20	2	18	31	-0.15
mmu-miR-2861	2.49E-01	260	84	179	12	-0.53
mmu-miR-3105-3p	2.50E-01	36	3	7	8	-2.32
mmu-miR-2137	2.52E-01	252	15	267	6	0.08
mmu-miR-547-5p	2.52E-01	29	31	63	14	1.12
mmu-miR-1912-3p	2.53E-01	6	6	47	33	2.87
mmu-miR-880-5p	2.55E-01	0	0	22	38	7.69
mmu-miR-217-5p	2.55E-01	24	17	56	26	1.25
mmu-miR-1930-3p	2.55E-01	14	12	93	12	2.74
mmu-miR-31-5p	2.56E-01	51	7	10	11	-2.37
mmu-miR-3474	2.60E-01	15	14	102	29	2.73
mmu-miR-129-1-3p	2.61E-01	1	2	39	55	5.00
mmu-miR-3113-5p	2.61E-01	69	2	31	42	-1.18
mmu-miR-210-3p	2.61E-01	72	19	12	11	-2.57
mmu-miR-15a-5p	2.61E-01	127	15	142	7	0.16
mmu-miR-185-5p	2.62E-01	11	1	11	19	-0.04
mmu-miR-129-2-3p	2.62E-01	1	3	49	45	5.04
mmu-miR-376b-3p	2.62E-01	75	14	92	16	0.29
mmu-miR-1934-3p	2.63E-01	14	17	82	45	2.56
mmu-miR-504-3p	2.63E-01	62	12	44	18	-0.51
mmu-let-7a-2-3p	2.64E-01	26	7	29	51	0.19
mmu-miR-127-3p	2.66E-01	52	9	79	29	0.60
mmu-miR-874-5p	2.67E-01	52	11	104	55	1.00
mmu-miR-3059-3p	2.67E-01	52	5	35	16	-0.59
mmu-miR-34a-3p	2.68E-01	2	3	48	66	4.96
mmu-miR-3473c	2.68E-01	2	3	90	134	5.63
mmu-miR-190b-3p	2.69E-01	0	0	19	33	7.14
mmu-miR-1961	2.69E-01	32	7	43	74	0.40
mmu-miR-692	2.70E-01	52	9	11	11	-2.26
mmu-miR-678	2.70E-01	54	18	21	20	-1.40
mmu-miR-3108-3p	2.70E-01	14	4	16	28	0.15
mmu-miR-1934-5p	2.70E-01	2	3	58	71	4.99
mmu-miR-5710	2.71E-01	25	19	59	25	1.23
mmu-miR-3087-5p	2.71E-01	19	17	112	37	2.58
mmu-miR-497-3p	2.71E-01	58	23	27	26	-1.13
mmu-miR-383-5p	2.71E-01	24	17	4	4	-2.53
mmu-miR-24-2-5p	2.73E-01	36	49	82	54	1.19
mmu-miR-1231-5p	2.74E-01	106	7	92	14	-0.21

mmu-miR-6347	2.74E-01	90	10	62	29	-0.55
mmu-miR-1960	2.74E-01	53	7	27	45	-0.97
mmu-miR-1224-5p	2.75E-01	74	11	47	27	-0.66
mmu-miR-1965	2.76E-01	94	5	81	14	-0.22
mmu-miR-5615-5p	2.77E-01	2	4	82	71	5.13
mmu-miR-1927	2.77E-01	7	4	25	21	1.73
mmu-miR-6346	2.78E-01	59	35	29	11	-1.05
mmu-miR-1951	2.78E-01	92	17	30	46	-1.63
mmu-miR-466i-5p	2.79E-01	4,629	92	4,287	386	-0.11
mmu-miR-182-5p	2.79E-01	38	13	51	0	0.43
mmu-miR-3067-5p	2.79E-01	10	2	12	21	0.24
mmu-miR-669h-3p	2.80E-01	58	32	111	59	0.94
mmu-miR-666-5p	2.80E-01	58	13	75	20	0.38
mmu-miR-1963	2.81E-01	27	14	36	62	0.41
mmu-miR-467b-5p	2.82E-01	3	6	135	144	5.40
mmu-miR-3104-5p	2.82E-01	109	3	84	31	-0.36
mmu-miR-96-3p	2.83E-01	26	23	3	4	-2.96
mmu-miR-101a-5p	2.83E-01	16	5	21	37	0.42
mmu-miR-380-3p	2.84E-01	34	12	16	26	-1.10
mmu-miR-488-5p	2.86E-01	15	10	14	24	-0.06
mmu-miR-679-3p	2.86E-01	38	21	10	13	-1.92
mmu-miR-6238	2.87E-01	36	13	22	38	-0.67
mmu-miR-872-3p	2.89E-01	15	14	70	24	2.24
mmu-miR-466h-5p	2.89E-01	55	9	82	35	0.57
mmu-miR-1953	2.89E-01	38	15	65	113	0.80
mmu-miR-215-5p	2.90E-01	106	31	135	12	0.36
mmu-miR-3110-3p	2.90E-01	60	14	42	17	-0.52
mmu-miR-128-1-5p	2.90E-01	16	14	76	28	2.28
mmu-miR-1298-5p	2.91E-01	12	13	62	37	2.38
mmu-let-7c-1-3p	2.92E-01	16	9	21	37	0.42
mmu-miR-106b-3p	2.93E-01	14	8	19	32	0.38
mmu-miR-3109-5p	2.93E-01	14	7	19	32	0.43
mmu-miR-28a-3p	2.94E-01	39	34	4	4	-3.22
mmu-miR-193a-5p	2.95E-01	26	21	68	34	1.36
mmu-miR-192-3p	2.97E-01	22	22	46	23	1.07
mmu-miR-669d-2-3p	2.98E-01	3	6	72	87	4.41
mmu-miR-455-3p	2.98E-01	128	29	102	10	-0.32
mmu-miR-493-5p	3.00E-01	12	10	14	24	0.22
mmu-miR-3088-3p	3.00E-01	23	22	100	20	2.09
mmu-miR-5618-5p	3.01E-01	4	6	73	63	4.32
mmu-miR-141-3p	3.02E-01	197	52	44	42	-2.17
mmu-miR-30e-3p	3.02E-01	150	23	125	25	-0.26
mmu-miR-1950	3.02E-01	18	17	0	0	-9.50
mmu-miR-370-5p	3.03E-01	74	16	26	36	-1.54
mmu-miR-872-5p	3.03E-01	33	35	132	24	2.01
mmu-miR-669j	3.04E-01	44	24	12	14	-1.86
mmu-miR-3092-3p	3.05E-01	5	9	151	132	4.84
mmu-miR-362-3p	3.05E-01	16	11	23	39	0.46
mmu-miR-6413	3.05E-01	23	8	34	12	0.55

mmu-miR-546	3.06E-01	28	30	72	33	1.38
mmu-miR-1956	3.06E-01	139	32	75	52	-0.89
mmu-miR-6418-3p	3.07E-01	3	4	23	24	3.22
mmu-miR-6408	3.07E-01	11	2	18	32	0.75
mmu-miR-676-3p	3.07E-01	54	33	22	21	-1.32
mmu-miR-299a-5p	3.08E-01	46	6	41	2	-0.15
mmu-miR-3080-5p	3.08E-01	7	7	41	31	2.54
mmu-miR-1964-5p	3.09E-01	92	18	114	27	0.31
mmu-miR-764-3p	3.11E-01	4	7	62	56	3.90
mmu-miR-92b-3p	3.11E-01	43	30	79	27	0.88
mmu-miR-193a-3p	3.13E-01	5	9	98	86	4.22
mmu-miR-667-5p	3.15E-01	46	35	91	30	0.98
mmu-miR-3103-3p	3.16E-01	13	2	27	46	1.00
mmu-miR-485-5p	3.16E-01	28	22	31	53	0.11
mmu-miR-216b-5p	3.18E-01	4	7	46	42	3.47
mmu-miR-9-5p	3.18E-01	142	39	39	38	-1.88
mmu-miR-3968	3.19E-01	25	8	13	20	-0.95
mmu-miR-3074-5p	3.19E-01	3	5	19	17	2.74
mmu-miR-297a-3p	3.19E-01	18	17	59	6	1.74
mmu-miR-466o-3p	3.20E-01	4	7	36	39	3.24
mmu-miR-133a-3p	3.20E-01	76	20	30	43	-1.33
mmu-miR-142-5p	3.21E-01	30	24	32	55	0.10
mmu-miR-802-3p	3.21E-01	4	6	51	78	3.79
mmu-miR-377-5p	3.22E-01	47	9	14	13	-1.69
mmu-miR-301b-3p	3.22E-01	43	17	13	12	-1.73
mmu-miR-544-5p	3.23E-01	5	8	47	41	3.37
mmu-let-7f-1-3p	3.23E-01	38	7	13	13	-1.59
mmu-miR-744-3p	3.23E-01	10	9	14	24	0.47
mmu-miR-147-3p	3.24E-01	18	9	42	72	1.17
mmu-miR-6237	3.24E-01	73	20	22	21	-1.74
mmu-miR-29c-3p	3.24E-01	53	10	44	8	-0.27
mmu-miR-92b-5p	3.25E-01	40	29	73	21	0.84
mmu-miR-135a-5p	3.25E-01	5	9	53	47	3.41
mmu-miR-181b-5p	3.26E-01	96	10	75	27	-0.35
mmu-miR-547-3p	3.27E-01	4	7	47	66	3.43
mmu-miR-5627-5p	3.29E-01	82	23	111	33	0.45
mmu-miR-467h	3.29E-01	99	55	30	35	-1.72
mmu-miR-484	3.30E-01	36	30	30	52	-0.28
mmu-miR-291a-3p	3.30E-01	72	16	25	27	-1.54
mmu-miR-152-5p	3.31E-01	33	3	14	18	-1.21
mmu-miR-532-5p	3.31E-01	26	9	9	8	-1.55
mmu-miR-323-5p	3.32E-01	16	1	41	71	1.39
mmu-miR-1942	3.33E-01	6	10	54	60	3.23
mmu-miR-3544-5p	3.33E-01	8	14	110	96	3.75
mmu-miR-3093-3p	3.34E-01	14	15	74	56	2.35
mmu-miR-106a-3p	3.36E-01	7	5	11	19	0.64
mmu-miR-1964-3p	3.37E-01	60	10	21	21	-1.49
mmu-miR-133c	3.37E-01	5	9	38	38	2.85
mmu-miR-1954	3.37E-01	91	5	59	46	-0.61

mmu-miR-295-5p	3.38E-01	70	8	38	46	-0.89
mmu-miR-3070a-3p	3.40E-01	72	10	65	5	-0.15
mmu-miR-193b-5p	3.43E-01	19	16	63	34	1.74
mmu-miR-1958	3.43E-01	100	29	60	53	-0.74
mmu-miR-7a-1-3p	3.43E-01	4	7	20	22	2.26
mmu-miR-370-3p	3.45E-01	102	42	36	36	-1.52
mmu-miR-599	3.46E-01	60	4	22	19	-1.45
mmu-miR-598-3p	3.46E-01	66	18	26	29	-1.34
mmu-miR-671-3p	3.46E-01	87	28	31	29	-1.50
mmu-miR-135b-5p	3.47E-01	8	13	55	51	2.87
mmu-miR-654-3p	3.48E-01	20	19	68	41	1.73
mmu-miR-148a-5p	3.49E-01	57	25	27	23	-1.04
mmu-miR-362-5p	3.50E-01	84	28	30	28	-1.47
mmu-miR-767	3.51E-01	31	9	42	16	0.47
mmu-miR-3113-3p	3.53E-01	75	18	49	32	-0.61
mmu-miR-350-3p	3.54E-01	13	15	36	23	1.47
mmu-miR-493-3p	3.56E-01	92	17	37	39	-1.30
mmu-miR-345-5p	3.56E-01	15	13	47	34	1.64
mmu-miR-1190	3.56E-01	23	13	11	9	-1.01
mmu-miR-5623-3p	3.57E-01	14	12	36	15	1.41
mmu-miR-149-5p	3.57E-01	79	28	39	34	-1.01
mmu-miR-381-5p	3.58E-01	106	36	59	44	-0.84
mmu-miR-500-3p	3.58E-01	50	38	24	14	-1.07
mmu-miR-6415	3.59E-01	19	16	50	24	1.41
mmu-miR-6405	3.60E-01	41	15	16	14	-1.34
mmu-miR-431-5p	3.62E-01	35	11	23	34	-0.65
mmu-miR-3106-5p	3.63E-01	37	11	16	15	-1.21
mmu-miR-669d-5p	3.65E-01	102	31	43	43	-1.24
mmu-miR-15a-3p	3.65E-01	34	13	55	27	0.71
mmu-miR-324-3p	3.67E-01	32	18	13	14	-1.31
mmu-miR-30d-3p	3.67E-01	52	18	23	22	-1.18
mmu-miR-1249-5p	3.67E-01	17	15	44	22	1.36
mmu-miR-760-3p	3.68E-01	32	17	13	12	-1.33
mmu-miR-5120	3.68E-01	8	8	14	24	0.72
mmu-miR-1968-3p	3.68E-01	61	3	41	35	-0.58
mmu-miR-150-5p	3.69E-01	63	24	35	33	-0.85
mmu-miR-28c	3.69E-01	94	11	55	48	-0.78
mmu-miR-471-3p	3.70E-01	1	1	19	33	4.88
mmu-miR-133b-3p	3.71E-01	61	44	25	28	-1.29
mmu-miR-153-3p	3.71E-01	34	20	14	16	-1.28
mmu-miR-93-3p	3.72E-01	27	23	62	37	1.21
mmu-miR-5621-5p	3.73E-01	69	33	92	8	0.41
mmu-miR-344d-3p	3.73E-01	1	1	23	40	5.05
mmu-miR-27a-5p	3.73E-01	70	35	29	27	-1.28
mmu-miR-1970	3.74E-01	44	14	20	18	-1.14
mmu-miR-199a-5p	3.74E-01	96	1	83	22	-0.21
mmu-miR-673-3p	3.75E-01	57	22	25	22	-1.21
mmu-miR-1955-5p	3.75E-01	120	24	56	58	-1.09
mmu-miR-674-3p	3.76E-01	51	28	21	20	-1.28

mmu-let-7e-3p	3.76E-01	61	5	28	25	-1.10
mmu-miR-876-3p	3.78E-01	1	1	20	35	4.77
mmu-miR-344g-3p	3.79E-01	41	21	66	38	0.68
mmu-miR-466n-3p	3.79E-01	1	1	45	77	5.72
mmu-miR-3073a-5p	3.79E-01	7	6	23	26	1.77
mmu-miR-3102-5p.2-5p	3.80E-01	188	54	148	36	-0.35
mmu-miR-5709	3.83E-01	12	10	27	18	1.22
mmu-miR-141-5p	3.85E-01	15	25	59	70	2.01
mmu-miR-5130	3.85E-01	37	11	22	24	-0.77
mmu-miR-669b-3p	3.85E-01	1	2	123	212	6.83
mmu-miR-668-3p	3.86E-01	70	44	97	16	0.48
mmu-miR-5122	3.86E-01	44	4	23	20	-0.97
mmu-miR-184-5p	3.88E-01	1	2	64	110	5.95
mmu-miR-92a-1-5p	3.88E-01	16	17	41	32	1.37
mmu-miR-210-5p	3.89E-01	36	26	63	34	0.79
mmu-miR-17-3p	3.91E-01	38	16	20	21	-0.93
mmu-let-7a-1-3p	3.93E-01	73	10	39	36	-0.90
mmu-miR-99a-3p	3.93E-01	33	16	20	26	-0.73
mmu-miR-135a-1-3p	3.93E-01	40	41	79	37	0.97
mmu-miR-218-2-3p	3.95E-01	35	30	67	16	0.93
mmu-miR-880-3p	3.95E-01	1	2	40	69	5.25
mmu-miR-5115	3.95E-01	202	18	218	22	0.11
mmu-miR-296-3p	3.96E-01	94	11	71	43	-0.41
mmu-miR-203-3p	3.98E-01	22	17	32	5	0.55
mmu-miR-669e-5p	3.99E-01	96	39	51	49	-0.92
mmu-miR-882	4.00E-01	49	11	39	56	-0.32
mmu-miR-150-3p	4.01E-01	73	21	43	46	-0.76
mmu-miR-298-5p	4.03E-01	77	8	59	29	-0.38
mmu-miR-434-3p	4.03E-01	35	5	20	18	-0.79
mmu-miR-101c	4.04E-01	16	10	14	21	-0.20
mmu-miR-30b-3p	4.05E-01	80	52	40	36	-1.02
mmu-miR-718	4.06E-01	27	15	14	12	-0.99
mmu-miR-592-3p	4.06E-01	38	35	67	20	0.80
mmu-miR-135a-2-3p	4.06E-01	51	45	88	51	0.78
mmu-miR-3098-5p	4.06E-01	27	18	22	33	-0.30
mmu-miR-669k-3p	4.07E-01	66	46	31	30	-1.09
mmu-miR-138-2-3p	4.07E-01	40	6	25	24	-0.71
mmu-miR-3112-5p	4.08E-01	6	6	13	22	1.11
mmu-let-7i-3p	4.10E-01	57	28	30	26	-0.92
mmu-miR-1945	4.10E-01	92	20	55	48	-0.76
mmu-miR-146a-5p	4.11E-01	90	51	126	30	0.49
mmu-miR-18a-5p	4.13E-01	6	4	22	37	1.77
mmu-miR-3100-3p	4.14E-01	118	45	85	17	-0.48
mmu-miR-5620-5p	4.15E-01	43	37	69	25	0.67
mmu-miR-23a-5p	4.16E-01	30	28	47	14	0.67
mmu-miR-27b-5p	4.18E-01	55	45	21	18	-1.39
mmu-miR-551b-3p	4.18E-01	36	18	23	24	-0.65
mmu-miR-298-3p	4.18E-01	29	9	18	16	-0.67
mmu-miR-3077-5p	4.21E-01	94	14	82	16	-0.20

mmu-miR-3110-5p	4.21E-01	33	7	21	19	-0.63
mmu-miR-139-5p	4.24E-01	106	46	68	50	-0.65
mmu-miR-1188-5p	4.25E-01	193	41	217	1	0.16
mmu-miR-763	4.27E-01	2	3	32	56	4.32
mmu-miR-211-3p	4.28E-01	8	6	28	49	1.91
mmu-miR-1943-5p	4.28E-01	78	7	55	50	-0.51
mmu-miR-96-5p	4.29E-01	39	17	27	28	-0.54
mmu-miR-1948-5p	4.32E-01	43	29	24	23	-0.82
mmu-miR-16-1-3p	4.33E-01	55	25	73	23	0.40
mmu-miR-5621-3p	4.34E-01	27	24	42	22	0.63
mmu-miR-22-5p	4.35E-01	62	79	70	22	0.18
mmu-miR-205-5p	4.36E-01	63	7	45	38	-0.48
mmu-miR-125a-3p	4.39E-01	13	1	13	19	0.07
mmu-miR-470-3p	4.40E-01	2	4	50	86	4.53
mmu-miR-138-5p	4.43E-01	54	26	38	34	-0.49
mmu-miR-299b-5p	4.44E-01	34	2	26	23	-0.37
mmu-miR-19b-1-5p	4.47E-01	22	11	18	22	-0.26
mmu-miR-451b	4.48E-01	10	1	14	22	0.55
mmu-miR-132-5p	4.48E-01	3	5	111	192	5.21
mmu-miR-452-5p	4.50E-01	6	4	27	46	2.21
mmu-miR-667-3p	4.50E-01	23	10	42	26	0.89
mmu-miR-98-5p	4.50E-01	46	23	37	40	-0.32
mmu-miR-1967	4.51E-01	66	11	49	36	-0.44
mmu-miR-3095-5p	4.51E-01	2	4	20	35	3.30
mmu-miR-3096b-3p	4.54E-01	42	36	55	23	0.39
mmu-miR-6418-5p	4.54E-01	161	8	174	23	0.11
mmu-miR-143-5p	4.56E-01	64	44	42	37	-0.60
mmu-miR-204-3p	4.58E-01	24	9	22	26	-0.13
mmu-miR-1907	4.58E-01	80	10	90	18	0.17
mmu-miR-344d-1-5p	4.64E-01	21	4	37	22	0.81
mmu-miR-543-3p	4.64E-01	36	31	42	12	0.21
mmu-miR-471-5p	4.67E-01	3	6	47	81	3.87
mmu-miR-140-5p	4.70E-01	28	11	29	35	0.03
mmu-miR-466l-5p	4.71E-01	4	6	66	61	4.13
mmu-miR-1943-3p	4.71E-01	80	19	76	66	-0.08
mmu-miR-468-5p	4.73E-01	3	6	34	60	3.42
mmu-miR-2139	4.74E-01	15	13	22	18	0.57
mmu-miR-221-3p	4.75E-01	272	33	255	1	-0.09
mmu-miR-744-5p	4.77E-01	32	16	29	39	-0.13
mmu-miR-93-5p	4.79E-01	123	31	144	30	0.22
mmu-miR-140-3p	4.80E-01	140	30	112	63	-0.32
mmu-miR-365-2-5p	4.80E-01	56	44	41	41	-0.43
mmu-miR-361-3p	4.80E-01	4	6	38	66	3.38
mmu-miR-151-3p	4.80E-01	63	11	49	34	-0.36
mmu-miR-582-3p	4.81E-01	27	24	29	10	0.08
mmu-miR-136-3p	4.83E-01	4	7	59	101	3.76
mmu-miR-665-5p	4.85E-01	56	34	44	43	-0.37
mmu-miR-1957a	4.89E-01	74	14	59	53	-0.31
mmu-miR-879-3p	4.91E-01	30	12	31	33	0.06

mmu-miR-878-3p	4.92E-01	44	15	46	40	0.06
mmu-miR-3080-3p	4.95E-01	48	2	83	48	0.78
mmu-miR-1948-3p	4.95E-01	48	25	48	42	0.00
mmu-miR-291b-5p	4.98E-01	97	78	61	59	-0.66
mmu-miR-669i	5.02E-01	60	50	40	50	-0.57
mmu-miR-7b-5p	5.04E-01	10	14	27	42	1.41
mmu-miR-532-3p	5.06E-01	30	7	24	14	-0.33
mmu-miR-3072-5p	5.06E-01	141	13	150	16	0.09
mmu-miR-195b	5.07E-01	35	28	37	49	0.08
mmu-miR-1946b	5.08E-01	83	30	62	40	-0.41
mmu-miR-7a-2-3p	5.08E-01	21	21	36	35	0.76
mmu-miR-883b-5p	5.09E-01	34	3	41	36	0.26
mmu-miR-25-3p	5.11E-01	402	106	446	34	0.15
mmu-miR-6409	5.13E-01	29	5	24	20	-0.26
mmu-miR-3103-5p	5.18E-01	49	22	43	52	-0.18
mmu-miR-367-5p	5.20E-01	25	31	39	39	0.65
mmu-miR-1971	5.24E-01	42	4	34	20	-0.27
mmu-miR-1947-3p	5.30E-01	99	19	82	45	-0.27
mmu-miR-139-3p	5.31E-01	105	45	84	72	-0.32
mmu-miR-344f-5p	5.33E-01	3	1	29	50	3.22
mmu-miR-453	5.33E-01	15	10	16	16	0.04
mmu-miR-3090-5p	5.33E-01	40	11	56	49	0.47
mmu-miR-224-3p	5.33E-01	87	75	63	23	-0.47
mmu-miR-770-3p	5.34E-01	24	8	33	31	0.43
mmu-miR-470-5p	5.37E-01	54	46	61	60	0.17
mmu-miR-883a-5p	5.37E-01	29	15	43	56	0.58
mmu-miR-1982-5p	5.38E-01	34	24	47	23	0.46
mmu-miR-194-2-3p	5.40E-01	53	41	56	48	0.06
mmu-miR-455-5p	5.49E-01	17	17	16	15	-0.09
mmu-miR-187-3p	5.53E-01	58	5	52	20	-0.16
mmu-miR-3075-3p	5.56E-01	1	1	18	29	4.44
mmu-miR-5134-5p	5.65E-01	23	21	27	14	0.27
mmu-miR-344-5p	5.66E-01	7	2	22	36	1.59
mmu-miR-196b-5p	5.67E-01	39	5	43	10	0.16
mmu-miR-1946a	5.72E-01	108	28	92	42	-0.23
mmu-miR-194-5p	5.75E-01	233	11	220	39	-0.09
mmu-miR-5622-3p	5.79E-01	33	26	32	34	-0.07
mmu-miR-212-3p	5.80E-01	18	11	24	25	0.46
mmu-miR-361-5p	5.82E-01	125	57	96	45	-0.38
mmu-miR-92a-3p	5.82E-01	138	13	159	43	0.21
mmu-miR-15b-5p	5.83E-01	212	36	230	35	0.12
mmu-miR-299a-3p	5.85E-01	79	11	73	18	-0.13
mmu-miR-3079-5p	5.94E-01	3	2	19	33	2.61
mmu-miR-1199-3p	5.96E-01	36	6	41	12	0.21
mmu-miR-881-5p	5.97E-01	1	1	48	83	6.46
mmu-miR-3069-3p	5.98E-01	1	1	23	40	4.81
mmu-miR-1249-3p	6.00E-01	12	4	29	41	1.32
mmu-miR-292-3p	6.02E-01	54	47	32	44	-0.73
mmu-miR-24-3p	6.03E-01	749	89	714	46	-0.07

mmu-miR-23b-3p	6.03E-01	1,709	105	1,754	89	0.04
mmu-miR-3091-5p	6.05E-01	36	18	75	65	1.03
mmu-miR-339-3p	6.06E-01	29	27	28	15	-0.07
mmu-miR-3107-3p	6.07E-01	107	34	91	36	-0.23
mmu-miR-339-5p	6.12E-01	7	6	12	20	0.81
mmu-miR-137-3p	6.13E-01	8	8	46	80	2.58
mmu-miR-411-3p	6.18E-01	62	28	70	18	0.18
mmu-miR-465c-5p	6.23E-01	4	5	32	35	3.16
mmu-miR-467c-5p	6.23E-01	26	5	63	55	1.25
mmu-miR-758-3p	6.27E-01	20	15	23	34	0.18
mmu-miR-6407	6.29E-01	31	27	33	14	0.07
mmu-miR-135b-3p	6.37E-01	31	29	55	49	0.83
mmu-miR-1900	6.38E-01	2	3	16	28	2.69
mmu-miR-5136	6.39E-01	6	6	34	59	2.61
mmu-miR-875-3p	6.50E-01	4	4	39	34	3.27
mmu-let-7g-3p	6.54E-01	92	31	81	36	-0.19
mmu-miR-665-3p	6.54E-01	83	62	88	20	0.08
mmu-miR-1892	6.55E-01	104	12	97	28	-0.10
mmu-miR-27a-3p	6.55E-01	242	21	234	17	-0.05
mmu-miR-3089-3p	6.60E-01	5	7	50	49	3.19
mmu-miR-300-3p	6.66E-01	26	11	24	21	-0.12
mmu-miR-138-1-3p	6.69E-01	46	18	40	28	-0.17
mmu-miR-1947-5p	6.71E-01	97	32	89	57	-0.13
mmu-miR-125b-2-3p	6.85E-01	12	3	33	28	1.48
mmu-miR-540-3p	6.86E-01	7	11	15	19	1.17
mmu-miR-3090-3p	6.98E-01	25	20	67	58	1.43
mmu-miR-5627-3p	7.06E-01	70	37	81	33	0.21
mmu-miR-5622-5p	7.08E-01	2	2	18	29	3.28
mmu-miR-3091-3p	7.10E-01	6	6	51	46	3.02
mmu-miR-125b-1-3p	7.15E-01	11	4	37	34	1.72
mmu-miR-3106-3p	7.21E-01	20	23	14	25	-0.49
mmu-miR-5046	7.25E-01	67	47	49	9	-0.46
mmu-miR-34c-5p	7.28E-01	42	40	36	30	-0.21
mmu-miR-1968-5p	7.31E-01	34	9	36	5	0.07
mmu-miR-199b-5p	7.36E-01	45	9	43	23	-0.07
mmu-miR-497-5p	7.38E-01	77	22	70	8	-0.13
mmu-miR-34b-5p	7.42E-01	17	19	9	10	-0.92
mmu-miR-134-3p	7.43E-01	58	40	68	42	0.22
mmu-miR-193b-3p	7.44E-01	28	9	79	68	1.48
mmu-miR-378b	7.48E-01	181	48	188	10	0.05
mmu-miR-124-3p	7.54E-01	29	9	26	6	-0.13
mmu-miR-543-5p	7.54E-01	8	11	28	25	1.75
mmu-miR-100-5p	7.64E-01	55	10	60	20	0.13
mmu-miR-23b-5p	7.67E-01	15	23	50	50	1.69
mmu-miR-467a-5p	7.67E-01	17	14	58	51	1.77
mmu-miR-877-5p	7.69E-01	81	43	82	59	0.01
mmu-miR-133a-5p	7.69E-01	13	17	51	58	2.03
mmu-miR-5133	7.73E-01	40	24	46	23	0.21
mmu-miR-346-5p	7.74E-01	71	12	69	31	-0.04

mmu-miR-883a-3p	7.76E-01	11	10	14	24	0.41
mmu-miR-24-1-5p	7.81E-01	34	33	50	55	0.53
mmu-miR-486-3p	7.83E-01	282	105	296	67	0.07
mmu-miR-664-5p	7.84E-01	119	53	102	10	-0.22
mmu-miR-291b-3p	7.85E-01	16	14	32	56	1.06
mmu-miR-6410	7.86E-01	15	2	17	16	0.18
mmu-miR-487b-3p	7.89E-01	29	26	5	6	-2.56
mmu-miR-153-5p	7.90E-01	49	7	48	22	-0.03
mmu-miR-9-3p	7.96E-01	10	10	19	33	0.84
mmu-miR-879-5p	7.96E-01	10	8	35	33	1.78
mmu-miR-3089-5p	7.99E-01	10	4	50	44	2.31
mmu-miR-3097-3p	8.01E-01	27	33	23	32	-0.25
mmu-miR-5131	8.02E-01	33	24	29	7	-0.19
mmu-miR-369-3p	8.03E-01	9	10	13	22	0.50
mmu-miR-499-3p	8.07E-01	75	51	72	23	-0.06
mmu-miR-3092-5p	8.12E-01	17	16	65	57	1.96
mmu-miR-877-3p	8.13E-01	12	17	26	22	1.08
mmu-miR-6416-5p	8.14E-01	1	1	17	30	4.10
mmu-miR-669d-3p	8.16E-01	13	14	39	35	1.63
mmu-miR-5626-5p	8.18E-01	7	6	12	21	0.85
mmu-miR-128-3p	8.19E-01	25	21	55	47	1.16
mmu-miR-669h-5p	8.20E-01	14	15	38	65	1.40
mmu-miR-99a-5p	8.38E-01	203	33	206	15	0.02
mmu-miR-92a-2-5p	8.38E-01	27	17	57	48	1.08
mmu-miR-1199-5p	8.39E-01	37	15	34	10	-0.14
mmu-miR-16-2-3p	8.43E-01	24	12	38	28	0.63
mmu-miR-3075-5p	8.45E-01	46	16	50	24	0.14
mmu-miR-99b-3p	8.48E-01	65	55	50	35	-0.38
mmu-miR-713	8.53E-01	1	1	32	55	4.55
mmu-miR-666-3p	8.60E-01	86	32	95	38	0.13
mmu-miR-467d-5p	8.62E-01	34	34	109	94	1.69
mmu-miR-759	8.62E-01	4	4	13	17	1.61
mmu-miR-483-3p	8.63E-01	29	41	55	68	0.95
mmu-miR-134-5p	8.72E-01	22	21	61	62	1.44
mmu-miR-669g	8.76E-01	20	23	37	32	0.91
mmu-miR-764-5p	8.82E-01	1	1	24	42	4.09
mmu-miR-542-5p	8.84E-01	19	8	31	26	0.69
mmu-miR-378a-3p	8.85E-01	208	38	210	3	0.01
mmu-miR-345-3p	8.85E-01	13	12	38	55	1.51
mmu-miR-3096a-3p	8.89E-01	23	33	29	26	0.33
mmu-miR-540-5p	8.89E-01	15	15	25	22	0.79
mmu-miR-124-5p	8.92E-01	18	1	23	17	0.33
mmu-miR-7a-5p	8.92E-01	22	28	31	27	0.53
mmu-miR-294-5p	8.95E-01	36	31	20	29	-0.87
mmu-miR-224-5p	9.00E-01	19	31	12	11	-0.64
mmu-miR-299b-3p	9.00E-01	46	28	42	19	-0.14
mmu-miR-145a-3p	9.02E-01	8	8	38	66	2.29
mmu-miR-3077-3p	9.04E-01	12	11	21	24	0.80
mmu-miR-196a-2-3p	9.05E-01	36	9	36	9	-0.03

mmu-miR-669m-3p	9.19E-01	24	22	42	37	0.80
mmu-miR-1306-3p	9.20E-01	15	20	38	33	1.36
mmu-miR-293-3p	9.21E-01	28	24	22	35	-0.33
mmu-miR-365-3p	9.32E-01	19	18	26	30	0.51
mmu-miR-664-3p	9.39E-01	16	24	13	20	-0.25
mmu-miR-1957b	9.44E-01	42	45	29	41	-0.56
mmu-miR-365-1-5p	9.50E-01	24	24	12	11	-0.99
mmu-miR-152-3p	9.54E-01	201	60	193	9	-0.06
mmu-let-7a-5p	9.59E-01	2,583	74	2,590	134	0.00
mmu-miR-146b-3p	9.60E-01	32	28	24	30	-0.44
mmu-miR-3096b-5p	9.64E-01	26	23	35	41	0.41
mmu-miR-369-5p	9.67E-01	16	20	15	21	-0.07
mmu-miR-367-3p	9.68E-01	18	20	19	31	0.05
mmu-miR-195a-3p	9.76E-01	116	46	112	41	-0.04
mmu-miR-20b-5p	9.77E-01	20	4	31	24	0.64
mmu-miR-3096a-5p	9.78E-01	48	45	37	35	-0.37
mmu-miR-144-3p	9.81E-01	22	24	15	19	-0.53
mmu-miR-145b	9.81E-01	33	29	28	31	-0.26
mmu-miR-3067-3p	9.83E-01	22	9	24	14	0.12
mmu-miR-185-3p	9.83E-01	4	6	16	27	1.95
mmu-miR-876-5p	9.85E-01	3	4	13	22	2.08
mmu-miR-696	9.85E-01	44	21	41	16	-0.08
mmu-miR-1893	9.86E-01	27	9	30	15	0.14
mmu-miR-467e-5p	9.88E-01	7	10	43	74	2.59
mmu-miR-146b-5p	9.90E-01	27	25	26	35	-0.06
mmu-miR-218-1-3p	9.91E-01	3	2	25	44	3.24
mmu-miR-322-3p	9.92E-01	59	5	65	31	0.12
mmu-miR-30a-3p	9.93E-01	133	78	115	35	-0.21
mmu-miR-101b-3p	9.96E-01	25	25	24	31	-0.05
mmu-miR-1949	9.98E-01	38	41	30	28	-0.33
mmu-miR-466d-5p	9.99E-01	82	21	83	26	0.01

Supplementary Figure 4: miRNA RT-PCR Primers

miRNA	Nephron segment	miScript specific Primers	Efficiency
RNU6-6P	Endogenous	RNA, U6 small nuclear 6, pseudogene	0.96 ± 0.04
SNORD61	Endogenous	SNORD61 small nucleolar RNA, C/D box 61	0.95 ± 0.04
miR-143-3p	Gl	5'UGAGAUGAAGCACUGUAGCUC	0.94 ± 0.04
miR-195a-5p	Gl	5'UAGCAGCACAGAAAUAUUGGC	0.96 ± 0.03
miR-107-3p	PCT/PST	5'AGCAGCAUUGUACAGGGCUAUCA	0.97 ± 0.04
miR-34a-5p	PCT/PST	5'UGGCAGUGUCUUAGCUGGUUGU	0.98 ± 0.03
miR-193b-3p	TAL	5'AACUGGCCCACAAAGUCCCGCU	0.96 ± 0.04
miR-378a-5p	TAL	5'CUCCUGACUCCAGGUCCUGUGU	0.98 ± 0.04
miR-874-3p	DCT	5'CUGCCCUGGCCCGAGGGACCGA	0.95 ± 0.04
miR-155-5p	DCT	5'UUAAUGCUAAUUGUGAUAGGGGU	0.96 ± 0.03
miR-200c-3p	CD	5'UAAUACUGCCGGGUAAUGAUGGA	0.96 ± 0.04
miR-96-5p	CD	5'UUUGGCACUAGCACAUUUUUGCU	0.98 ± 0.03

SIGNIFICANCE STATEMENT

microRNAs (miRNAs), short, non-coding RNAs that inhibit mRNA translation, have been shown to be downregulated in tubulointerstitial fibrosis (TIF), yet they appear to be dispensable for proximal tubule function. This study reports that proximal tubules and collecting ducts exhibit distinct miRNA expression profiles. Suppression of miRNAs in collecting ducts, using three mouse models that lack key enzymes needed for miRNA function, spontaneously induces partial epithelial-to-mesenchymal transition (EMT) and results in progressive TIF and renal failure. Thus, downregulation of collecting duct-enriched miRNAs and the subsequent induction of partial EMT may be a new mechanism for TIF. The results suggest that the collecting duct may play a pivotal role in TIF initiation and progression.